ELSEVIER

Neurobiology of Disease

www.elsevier.com/locate/ynbdi
Neurobiology of Disease xx (2006) xxx - xxx

Modified expression of Mts1/S100A4 protein in C6 glioma cells or surrounding astrocytes affects migration of tumor cells *in vitro* and *in vivo*

Keizo Takenaga,[a,b] Jim Nygren,[a] Marina Zelenina,[c] Miki Ohira,[d] Toshihiko Iuchi,[e] Eugen Lukanidin,[f] Mats Sjöquist,[g] and Elena N. Kozlova[a,*]

[a]*Department of Neuroscience, Biomedical Center, Box 587, Uppsala University, 751 23 Uppsala, Sweden*
[b]*Division of Chemotherapy, Chiba Cancer Center Research Institute, 666-2 Nitona, Chuoh-ku, Chiba, 260-8717 Chiba, Japan*
[c]*Department of Woman and Child Health, Karolinska Institutet, 171 76 Stockholm, Sweden*
[d]*Division of Biochemistry, Chiba Cancer Center Research Institute, 666-2 Nitona, Chuoh-ku, Chiba, 260-8717 Chiba, Japan*
[e]*Division of Neurological Surgery, Chiba Cancer Center, 666-2 Nitona, Chuoh-ku, Chiba, 260-8717 Chiba, Japan*
[f]*Danish Cancer Society, Department of Molecular Cancer Biology, Strandboulevarden 49, DK-2100 Copenhagen, Denmark*
[g]*Department of Medical Cell Biology, Biomedical Center, Uppsala University, Box 572, 751 23 Uppsala, Sweden*

Received 27 June 2006; revised 12 October 2006; accepted 19 October 2006

The calcium-binding Mts1/S100A4 protein plays an important role in motility and metastatic activity of tumor cells. Recently we showed that Mts1/S100A4 is expressed in white matter astrocytes and influences their migration *in vitro* and *in vivo*. Here, we have investigated the role of Mts1/S100A4 expression in C6 glioma cells or surrounding astrocytes for migration of C6 cells on astrocytes, using short interference (si) RNA to silence Mts1/S100A4 expression. We find that *in vitro*, the migration of Mts1/S100A4 expressing and silenced C6 cells on astrocytes is predominantly dependent on the expression of Mts1/S100A4 in astrocytes, i.e. C6 cells preferably migrate on Mts1/S100A4-silenced astrocytes. *In vivo*, Mts1/S100A4-positive C6 cells preferably migrate in white matter. In contrast Mts1/S100A4-silenced C6 cells avoid white matter and migrate in gray matter and meninges. Thus, the migration pattern of C6 cells is affected by their intrinsic Mts1/S100A4 expression as well as Mts1/S100A4 expression in astrocytes.

To investigate if Mts1/S100A4 has a significant role on brain tumor progression, we made quantitative RT-PCR analysis for the expression of S100A4/Mts1 in various grades of astrocytic tumors. Our data showed that high-grade glioblastomas express higher amount of S100A4/Mts1 than low-grade astrocytic tumors.

Keywords: White matter; Cell motility; Brain tumor; Transplantation; siRNA

Introduction

Diffuse astrocytomas are the most common primary intracranial tumors in humans. The rapid and uncontrolled spread of the tumors usually leads to the death of the patients within a short period after diagnosis. These tumors invade the brain preferentially along white matter fiber tracts (Pedersen et al., 1995; Giese et al., 1996; Kleihues and Cavanee, 1997). It is intriguing that although CNS myelin is inhibitory for neurite outgrowth (Bandtlow and Schwab, 2000), as well as for spreading and migration of several cell types including astrocytes and fibroblasts (Schwab and Caroni, 1988; Amberger et al., 1994; Spillmann et al., 1997), many cell types, including malignant cells, migrate readily in white matter areas (Amberger et al., 1998; Belien et al., 1999; Guillamo et al., 2001; Hormigo et al., 2001; Lefranc et al., 2005).

C6 rat glioma cells, a chemically induced highly invasive cell line (Benda et al., 1968), as well as human glioma cells are able to overcome the inhibitory properties of CNS myelin, and spread and migrate on CNS myelin substrate in culture due to the presence of a membrane-bound metalloprotease activity (C6-MP) (Paganetti et al., 1988; Amberger et al., 1994, 1998; Hensel et al., 1998). The expression of MT1-MMP on the surface of the C6 cell was associated with a remodeling of the non-permissive CNS myelin substrate into a permissive one, thereby allowing spreading, migration, and infiltration of glioma cells on a CNS myelin substrate *in vitro*, and their invasion of myelinated CNS fiber tracts *in vivo* (Belien et al., 1999). However, besides MT1-MMP, other properties of C6 cells could also be involved in overcoming the inhibitory properties of CNS myelin.

Mts1/S100A4 is a member of the EF-hand family of Ca-binding proteins, selectively expressed by white matter astrocytes in the intact CNS (Kozlova and Lukanidin, 1999; Åberg and Kozlova,

* Corresponding author. Department of Neuroscience, Neuroanatomy, Biomedical Center, Box 587, SE-751 23 Uppsala, Sweden. Fax: +46 18 55 90 17.
E-mail address: Elena.Kozlova@anatomi.uu.se (E.N. Kozlova).
Available online on ScienceDirect (www.sciencedirect.com).

0969-9961/$ - see front matter
doi:10.1016/j.nbd.2006.10.021

Please cite this article as: Takenaga, K., et al., Modified expression of Mts1/S100A4 protein in C6 glioma cells or surrounding astrocytes affects migration of tumor cells *in vitro* and *in vivo*, Neurobiol. Dis. (2006), doi:10.1016/j.nbd.2006.10.021

2000), and markedly up-regulated after injury (Kozlova and Lukanidin, 1999, 2002). Mts1/S100A4 is strongly implicated in invasion and metastasis of non-neural tumors (reviewed in Helfman et al., 2005). The protein is expressed in C6 glioma cells, but its function in these cells is unknown. Since Mts1/S100A4 is also expressed in white matter astrocytes *in vivo*, it is conceivable that the presence or absence of this protein in these cells influences how C6 glioma cells interact with white matter areas. Here, using siRNA mediated silencing of Mts1/S100A4, we first investigated the role of intracellular Mts1/S100A4 in C6 cells-white matter astrocytes interactions, especially focusing on *in vitro* migration of C6 cells. Subsequently, we examined whether Mts1/S100A4-expressing and -silenced C6 glioma cells migrate differently in CNS white matter *in vivo*.

Material and methods

Astrocyte cultures

The animal procedures were approved by the Uppsala county regional committee for research on animals. The detailed procedure for preparing cultures of astrocytes is described elsewhere (Kozlova and Takenaga, 2005). Briefly, white matter astrocytic cultures were made from 4 days old rat pups. The animals were anesthetized on ice and decapitated. The brain from 10 pups was removed, and placed in a Petri dish with cold PBS. A 2 mm thick coronal slice at the level of the rostral hippocampus was made and placed in a Petri dish with Dulbecco's modified Eagle's medium (DMEM; Gibco, Invitrogen) containing 10% FCS (Gibco, Invitrogen) supplemented with 100 units/ml penicillin and 100 μg/ml streptomycin. The corpus callosum area was carefully dissected at high magnification under the dissecting microscope, and used for obtaining white matter astrocytes. The tissues were rinsed with PBS containing 0.2% glucose (PBS/glucose), resuspended in PBS/glucose containing 10 mg/ml trypsin (Sigma-Aldrich, St. Louis, MO), 1 mg/ml DNase (Worthington Biochemicals Co., Lakewood, NJ), and 5 mg/ml $MgSO_4$, incubated for 3 min at 37 °C, and then carefully washed three times with PBS/glucose. After removing the last wash solution, they were suspended in DMEM containing 0.5 mg/ml DNase. Beginning with the 18-G needle, the tissues and the DNase solution were drawn up and expelled back for a total of fifteen times, and this procedure was repeated with the 20- and 23-G needles. The resulting cell suspension was centrifuged at 1200 g for 1 min, and the pellet was resuspended in 1 ml of a 1:1 mixture of DNase solution and PBS/glucose/$MgSO_4$. The cell suspension was transferred onto the discontinuous Percoll (Amersham Biosciences, Piscataway, NJ) gradient that had been made by overlaying 2.5 ml of 30% Percoll on 2.5 ml of 60% Percoll in PBS/glucose. After centrifugation at 2000×*g* for 10 min at 4 °C, the astrocyte-enriched fraction that migrated to the medium/30% Percoll interface was carefully aspirated with a Pasteur pipette, and suspended in 10 ml of PBS/glucose. The cells were centrifuged at 2000×*g* for 10 min at 4 °C, resuspended in DMEM/10% FCS/3% glutamine glucose, plated at a concentration of 2×10^5 cells/ml in culture flasks (T25), and then cultured for 10 days. For subculturing, the cells were incubated with 0.05% trypsin/0.53 mM EDTA (National Veterinary Institute, Uppsala, Sweden) for 3 min at 37 °C. After adding an equal volume of DMEM/10% FCS, the cells were detached from the culture flasks by smacking the side of the flasks, centrifuged, and resuspended in DMEM/10%FCS/glucose.

C6 glioma cell cultures

Rat glioma C6 cells (Namba et al., 2000) were cultured in Dulbecco's modified Eagle's medium (DMEM) containing 10% FCS supplemented with 100 units/ml penicillin and 100 μg/ml streptomycin. Enhanced green fluorescent protein (EGFP) expressing C6 (C6/EGFP) cells was established by introducing a pCI-neo/E9/EGFP plasmid with the Lipofectin (Invitrogen) method and selecting with 400 μg/ml G418 (Sigma-Aldrich) followed by cloning. Cells were cultured at 37 °C in a humidified atmosphere with 5% CO_2.

siRNA treatment

siRNA mediated silencing of endogenous expression of Mts1/S100A4 in C6 cells and astrocytes was performed using 21 nucleotide siRNA duplexes (Ambion Inc., Austin, TX). The sequence of sense and antisense oligonucleotide was 5′-GGGU-GACAAGUUCAAGCUGtt-3′ and 5′-CAGCUUGAACUUGU-CACCCtc-3′, respectively. S100A4 siRNA was transfected with Lipofectamine 2000 according to the manufacturer's instructions (Invitrogen). Briefly, 1 day before transfection, astrocytes and C6 cells were resuspended in 12-well plates in appropriate growth medium and then grown overnight. On the day of the experiment, siRNA–Lipofectamine 2000 complexes were prepared and transfection was performed according to the manufacturer's instructions. Medium for astrocytic cultures was changed to Opti-MEM (Invitrogen) 20 min before transfection. The siRNA complexes were added dropwise while gently rocking the 12-well plates. Cells were transfected with Mts1/S100A4 siRNA for at least 5 h at 37 °C before switching to fresh Opti-MEM containing 20% FCS and incubated overnight. The medium was then changed to DMEM supplemented with 3% glutamine, antibiotics (see above), and 10% FCS. The amounts of siRNA, Lipofectamine 2000 and siRNA transfection medium were proportionally scaled up to the surface area of cell culture. As a control for Mts1/S100A4 siRNA, BLOCK-iT Fluorescent Oligo (Invitrogen) or Silencer Negative Control #1 siRNA (Ambion, Inc.) was used. For co-culturing with C6 glioma cells, astrocytes that had been transfected with siRNA 2 days earlier were detached, immediately replated on glass coverslips and incubated for 24 h before C6 cells were plated on the top of astrocytes. After time-lapse microscopy, the cover slips were fixed and taken for immunohistochemical staining. Transfection efficiency was about 90% for astrocytes as well as C6 cells.

Astrocytic tumor specimens

Thirty astrocytic tumors of various grades (1 pilocytic astrocytomas, 5 diffuse astrocytomas, 10 anaplastic astrocytomas, 14 glioblastomas) were examined. All tissue samples were obtained from the patients at the Chiba Cancer Center Hospital under the protocol approved by the institutional review board. The histopathologic diagnoses of all specimens were confirmed by two pathologists according to the WHO criteria.

Real-time quantitative PCR analysis

Total RNA was extracted from the tumors according to the AGPC method (Chomczynski and Sacchi, 1987).

One microgram of each RNA was reverse transcribed using random primer (Takara Shuzo Co., Ltd., Japan) and Super Script II (Invitrogen Corp., Carlsbad, CA). Real-time quantitative PCR was

Please cite this article as: Takenaga, K., et al., Modified expression of Mts1/S100A4 protein in C6 glioma cells or surrounding astrocytes affects migration of tumor cells *in vitro* and *in vivo*, Neurobiol. Dis. (2006), doi:10.1016/j.nbd.2006.10.021

done using the ABI Prism 7700 Sequence Detector (Applied Biosystems). The TaqMan MGB probes for S100A4/Mts1 (FMA™ dye-labeled) (TaqMan(R) Gene Expression Assays, Assay ID: Hs XXXXX-m1) and TaqMan PCR Master Mix were used for amplification of human S100A4/Mts1. The real-time PCR condition was: 2 min at 50 °C, 10 min at 95 °C, and then 50 cycles of amplification for 15 s at 95 °C and 1 min at 60 °C. For each run, serial dilutions of human S100A4/Mts1 plasmids were used as standards for quantitative measurement of the amount of amplified DNA. In addition, for normalization of each sample, TaqMan GAPDH control reagent kit (Applied Biosystems) was used for the detection of GAPDH expression as a control. The ratios of S100A4/Mts1 and GAPDH gene expressions represented the normalized relative levels of S100A4/Mts1 expressions and were expressed as arbitrary expression units (a.e.u.).

Immunoblot

Cells were lysed in 2% Triton X-100, 1% Nonidet P-40, 20 mM Tris–HCl, pH 7.4, 300 mM NaCl, 2 mM EDTA, and 1 mM PMSF. After centrifugation at 10,000×*g* for 10 min at 4 °C, the supernatant was used for immunoblot analysis. Proteins were separated by SDS-PAGE under reducing conditions and transferred to a Hybond-N membrane (Amersham Biosciences). Primary antibodies used were against: β-actin (mouse monoclonal, Sigma-Aldrich, 1:1000), GFAP (rabbit polyclonal, DakoCytomation, Glostrup, Denmark, 1:100), and Mts1/S100A4 (rabbit polyclonal) (Takenaga et al., 1994). The membrane was blocked with 5% dry milk in TBS-T, incubated with the first antibodies, washed extensively with TBS-T, and then with species-appropriate horseradish peroxidase conjugated" secondary antibodies. Immunodetections of Mts1/S100A4, GFAP, and β-actin were made using the enhanced chemiluminescence system (ECL; Amersham Biosciences Corp., Piscataway, NJ).

Time-lapse microscopy

Just before the experiment, the C6/EGFP cells were harvested using 2 mM EDTA/PBS and 1×10^5 cells were added to a monolayer of astrocytes that had been cultured on a coverslip (diameter 40 mm) and placed in the middle of a 60-mm dish. The cells were kept in an incubator for 2 h, after which the coverslips with astrocytes and attached C6 cells were transferred to the closed chamber (Focht Live Cell Chamber System, Butler, PA) on the stage of a Zeiss 410 invert laser scanning microscope. The cells were scanned using a 63×/1.4 oil immersion objective. Fluorescence was excited by the argon laser line 488 nm and emitted fluorescence was detected using a bandpass filter at 515–525 nm. During the first hour, confocal images were recorded showing appearance of the attached C6/EGFP cells. Then a series of non-confocal images was recorded for the next 2 h with 5 min intervals between the images, to analyze C6 cell migration. The chamber temperature was kept at 37 °C throughout the experiment.

We analyzed three groups of experiments: (1) C6/EGFP cells (Mts1/S100A4 positive) cultured on Mts1/S100A4 positive astrocytes (C+W+), (2) C6/EGFP cells treated with Mts1/S100A4 siRNA (Mts1/S100A4 negative) cultured on Mts1/S100A4 positive astrocytes (C−W+), and (3) C6/EGFP cells (Mts1/S100A4 positive) cultured on astrocytes treated with Mts1/S100A4 siRNA (astrocytes Mts1/S100A4 negative) (C+W−). All images were analyzed with the ImageJ program. We calculated the distance covered by individual cells during an examination period of 2 h. The whole distance was calculated by the addition of all distances, which were recorded every 5 min during the 2-h experimental session. The data are presented in graphic form, and analyzed with the Student's *t*-test.

Quantitative analysis of C6 cell morphology

After time-lapse microscopy, the coverslips were carefully removed from the microscope chamber and fixed. Flat and round C6/EGFP cells in all 3 groups of co-cultures were visualized in the fluorescence microscope and counted on each coverslip under the 20× objective with the aid of a square ocular frame (side=0.11 mm). The frame was placed systematically across the coverslip. All together 11 frames were examined for each coverslip. At least 3 experiments were analyzed for each group. The data are presented in graphic form and analyzed with the Student's *t*-test.

Transplantation of C6/EGFP cells

A suspension of C6/EGFP cells was prepared just before transplantation. The recipient rats were placed in a stereotaxic holder and 5 μl of the suspension containing 1×10^5 C6/EGFP cells was injected with a thin metal tube with 50 μm diameter to the white matter areas with coordinates (0.8 mm back, 1.5 mm right, 3.7 mm down) from bregma. Four days later, the animals were perfused via the left ventricle with saline (37 °C), followed by a fixative solution containing 4% formaldehyde (w/v) and 14% saturated picric (v/v) acid in PBS (4–8 °C, pH 7.35–7.45). The brain was removed, postfixed for 4 h, and cryoprotected overnight in PBS containing 10% sucrose. Coronal sections (14 μm) were made on a cryostat. All sections through the entire transplant were collected, and subsequently used to reconstruct the rostro-caudal and medio-lateral extension of the transplant.

Immunohistochemistry

At the termination of the time-lapse microscopy session, all cultures were rinsed in PBS, fixed in 4% phosphate-buffered paraformaldehyde for 20 min, washed over night in PBS, and stained for GFAP and Mts1/S100A4. Cryostat sections from the brain of transplanted animals were thawed at room temperature until water condensations on the slides had disappeared. A blocking solution (1% bovine serum albumin [w/v], 0.3% Triton X-100, and 0.1% sodium azide in PBS) was gently put on top of each section for 1 h at room temperature. After blocking, the solution was removed and the sections treated overnight at 4 °C in the same solution with antibodies to Mts1/S100A4 (rabbit polyclonal, 1:700), or glial fibrillary acidic protein (GFAP; mouse monoclonal, 1:500, Jackson ImmunoResearch). The slides were washed three times in PBS (7 min/wash) and then incubated with secondary antibody. The immune complexes were visualized with Texas-red conjugated donkey anti-rabbit IgG (Jackson Immuno-Research Inc., West Grove, PA) diluted 1:50 in PBS with 0.3% Triton X-100 and 0.1% sodium azide for 4 h at room temperature. After another round of washing (three times, 7 min/rinse in PBS), the slides were mounted in a mixture of PBS and glycerol (1:1; v/v) containing 0.1 M propyl-gallate.

Microscopic analysis

For reconstruction of the transplants, the distance between the beginning and the end of each transplant was calculated by

Please cite this article as: Takenaga, K., et al., Modified expression of Mts1/S100A4 protein in C6 glioma cells or surrounding astrocytes affects migration of tumor cells *in vitro* and *in vivo*, Neurobiol. Dis. (2006), doi:10.1016/j.nbd.2006.10.021

counting the number of sections containing transplanted cells. Thereafter, we analyzed the width of the transplant, which was located in corpus callosum or in another parts of the brain, for example along the blood vessels or the meninges. In addition, we measured on transverse sections the maximal extension of each transplant to the contralateral side of the brain.

Total RNA preparation and reverse transcription-polymerase chain reaction (RT-PCR)

One microgram of total RNA which was prepared with TRIzol reagent (Invitrogen), was used as a template for cDNA synthesis. RNA was transcribed into cDNA as described previously (23) and the resulting cDNA was used for the amplification of the target cDNAs using the appropriate sense and antisense primers, and *r*Taq DNA polymerases (TOYOBO). The PCR conditions for matrix metalloproteinase (MMP)-2, MMP-9, membrane type (MT) 1-MMP, tissue inhibitor of metalloproteinases (TIMP)-1, and TIMP-2 were 94 °C for 10 s, 55 °C for 5 s, and 72 °C for 1 min, and the cycles were repeated 30 times except for an internal control glyceraldehyde 3-phosphate dehydrogenase (GAPDH; 25 cycles). Aliquots of the PCR products were fractionated by electrophoresis in 1% agarose gels and visualized on a transilluminator after staining with ethidium bromide. Oligonucleotide primers used for RT-PCR were as follows.

MMP-2	sense	5′-CTGGGTCTATTCTGCCAGCACTCTG-3′
	antisense	5′-AGCCAGTCTGATTTGATGCTTCCAA-3′
MMP-9	sense	5′-AGTTTGGTGTCGCGGAGCAC-3′
	antisense	5′-TACATGAGCGCTTCCGGCAC-3′
MT1-MMP	sense	5′-GTGCCCTATGCCTACATCCG-3′
	antisense	5′-TTGGGTATCCGTCCATCACT-3′
TIMP-1	sense	5′-CTGGCATCCTCTTGTTGCTA-3′
	antisense	5′-AGGGATCGCCAGGTGCACAA-3′
TIMP-2	sense	5′-AGACGTAGTGATCAGGGCCA-3′
	antisense	5′-GTACCACGCGCAAGAACCAT-3′
GAPDH	sense	5′-ACCACAGTCCATGCCATCAC-3′
	antisense	5′-TCCACCACCCTGTTGCTGTA-3′

Results

The objectives of our studies were to (i) explore whether the migration of C6 cells *in vitro* is influenced by astrocytes which express or do not express Mts1/S100A4, and (ii) determine whether intracellular Mts1/S100A4 in C6 glioma cells regulates their migratory properties *in vivo*. We produced cultures from the corpus callosum of postnatal day 4 (P4) old rats, i.e. the stage when Mts1/S100A4 positive astrocytes appear *in vivo* (Åberg and Kozlova, 2000), and used EGFP stably expressing cells established from a C6 glioma cell line (C6/EGFP) that expresses Mts1/S100A4. Using the siRNA technique to specifically eliminate Mts1/S100A4 protein expression, we were therefore able to examine the role of Mts1/S100A4 for the migratory capacity of C6 cells on white matter astrocytes expressing Mts1/S100A4 and on those with down-regulated expression.

Silencing of Mts1/S100A4 expression in white matter astrocytes and C6 cells

White matter astrocytes expressed high levels of Mts1/S100A4 and after transfection of Mts1/S100A4 siRNA an almost complete elimination of Mts1/S100A4 occurred on day three after transfection (Fig. 1A), consistent with our previous report (Kozlova and Takenaga, 2005). C6 glioma cells also expressed high levels of Mts1/S100A4, but were negative for GFAP. Transfection of Mts1/S100A4 siRNA into C6 cells resulted in a gradual depletion of Mts1/S100A4 immunoreactivity with an almost complete, concentration dependent disappearance on day three after transfection (Fig. 1B). C6 cells transfected with control siRNA showed no change in Mts1/S100A4 protein expression.

Morphology of C6 glioma cells on a monolayer of white matter astrocytes in vitro

C6/EGFP cells transfected with control or S100A4-specific siRNAs were placed on cultures of white matter astrocytes for a period of 4 h, after which their morphology was analyzed. Two distinct types of C6/EGFP cell shapes were observed: round and flat (extended). Most of the C6/EGFP cells, regardless of their Mts1/S100A4 expression demonstrated round morphology and did not extend on a monolayer of Mts1/S100A4-expressing white matter astrocytes (Figs. 2A, B). However, some of the C6/EGFP cells expressing Mts1/S100A4 partly extended on white matter astrocytes *in vitro* (Fig. 2A). Intriguingly, when C6/EGFP cells were seeded on a monolayer of Mts1/S100A4-silenced white matter astrocytes, most of the cells adopted a flat and extended shape (Figs. 2C, D). This change in C6/EGFP cell shape, induced by Mts1/S100A4-negative white matter astrocytes, occurred irrespective of whether C6 cells were treated with control siRNA or Mts1/S100A4 siRNA. These observations were confirmed by quantification of the number of flat and round C6/EGFP cells on white matter astrocytes expressing Mts1/S100A4 and white matter astrocytes with silenced Mts1/S100A4 expression (Fig. 2E). Thus, Mts1/S100A4 expressing C6/EGFP glioma cells were round on a monolayer of Mts1/S100A4-expressing astrocytes and flat on Mts1/S100A4 siRNA-treated white matter astrocytes.

Time-lapse microscopy

Mts1/S100A4-expressing or -silenced C6/EGFP cells were seeded for 2 h before the experiment on a monolayer of either Mts1/S100A4-expressing or -silenced white matter astrocytes. The

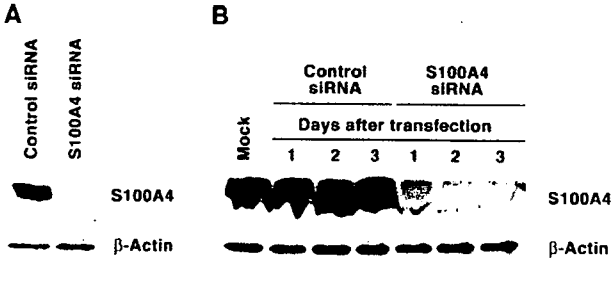

Fig. 1. The effect of Mts1/S100A4 siRNA on the expression of Mts1/S100A4 in C6 glioma cells. White matter astrocytes were transfected with 100 nM control siRNA or Mts1/S100A4 siRNA by the Lipofectamine 2000 method. Three days later, cell extracts (40 μg of protein) were prepared and subjected to immunoblot analysis of Mts1/S100A4 (A). C6 glioma cells were transfected with 100 nM control siRNA or Mts1/S100A4 siRNA. One to three days after the transfection, cell extracts (40 μg of protein) were prepared and subjected to immunoblot analysis of Mts1/S100A4 (B). β-actin was used as a loading control.

Please cite this article as: Takenaga, K., et al., Modified expression of Mts1/S100A4 protein in C6 glioma cells or surrounding astrocytes affects migration of tumor cells *in vitro* and *in vivo*, Neurobiol. Dis. (2006), doi:10.1016/j.nbd.2006.10.021

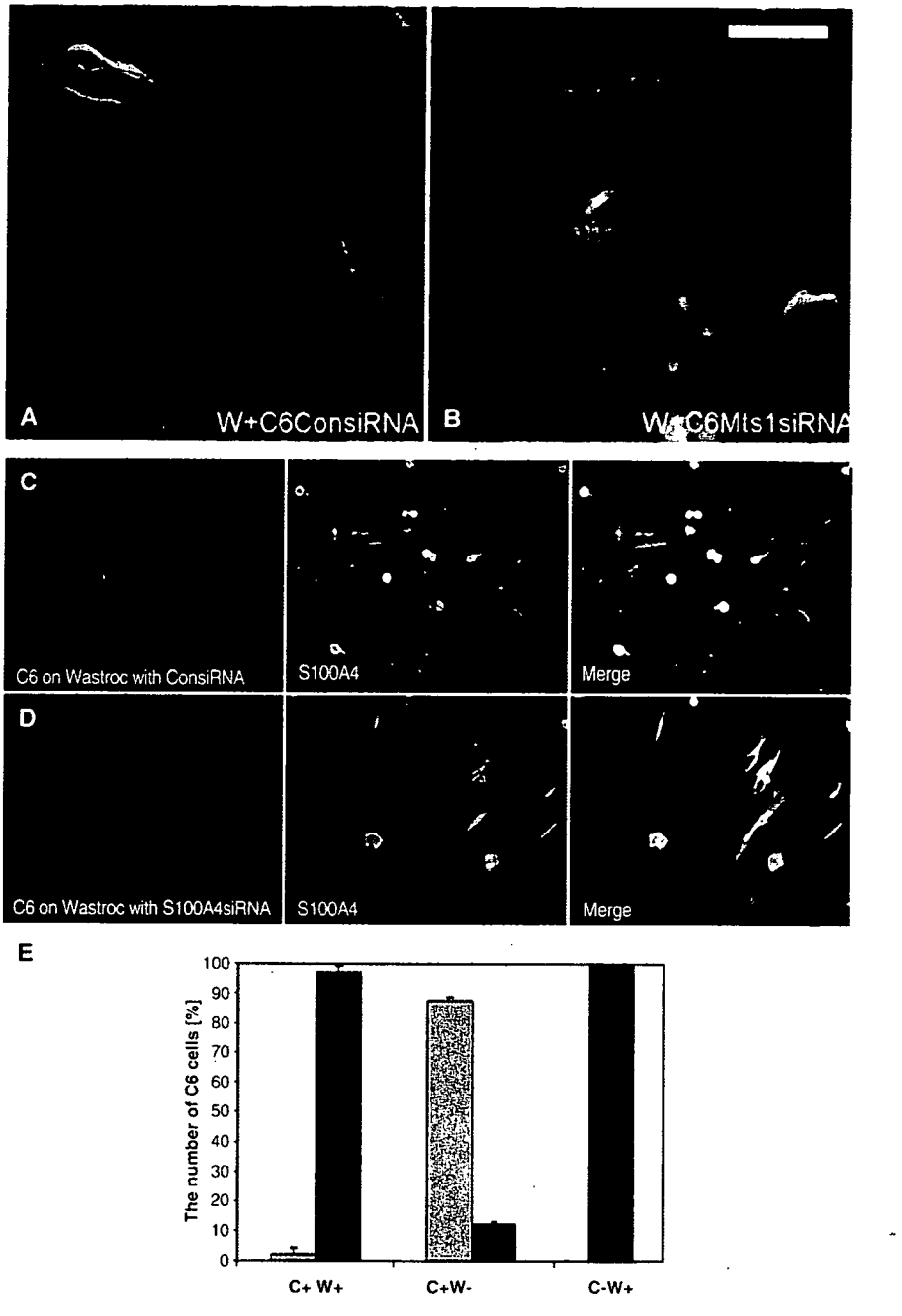

Fig. 2. Morphology of C6/EGFP cells on Mts1/S100A4-expressing white matter astrocytes (red) in confocal (A, B, and non-confocal (C, D) images. Regardless of whether C6 cells expressed Mts1/S100A4 or not, they typically showed a round shape on Mts1/S100A4 expressing white matter astrocytes (A–C). However, some of the C6/EGFP cells expressing Mts1/S100A4 partly extended on white matter astrocytes (A). When seeded on Mts1/S100A4-silenced white matter astrocytes, most of the C6/EGFP cells adopted a flat and extended shape (D). Quantitative analysis of the number of flat (gray bar) and round (black bar) Mts1/S100A4 positive (C+) and negative (C−) C6/EGFP cells on white matter astrocytes expressing Mts1/S100A4 (W+) or white matter astrocytes with silenced Mts1/S100A4 expression (W−) show that virtually all C6 cells display a round shape on Mts1/S100A4 expressing white matter astrocytes, whereas the vast majority of C6 cells are flat on Mts1/S100A4-silenced white matter astrocytes (E). Scale bar = 10 μm (A, B); 60 μm (C, D).

motility of C6/EGFP cells was recorded during a period of 2 h. We analyzed 3 different experiments: (1) C6/EGFP cells expressing Mts1/S100A4 seeded on astrocytes expressing Mts1/S100A4 (C+W+), (2) C6/EGFP cells with down-regulated Mts1/S100A4 seeded on astrocytes expressing Mts1/S100A4 (C−W+); (3) C6/EGFP cells expressing Mts1/S100A4 seeded on astrocytes with down-regulated Mts1/S100A4 (C+W−). The total distances of migratory movements for the three groups (C+W+, C−W+, and C+W−) were calculated in the ImageJ program and a graph was prepared in Excel using *t*-test (Fig. 3). Mts1/S100A4 positive C6/

Please cite this article as: Takenaga, K., et al., Modified expression of Mts1/S100A4 protein in C6 glioma cells or surrounding astrocytes affects migration of tumor cells *in vitro* and *in vivo*, Neurobiol. Dis. (2006), doi:10.1016/j.nbd.2006.10.021

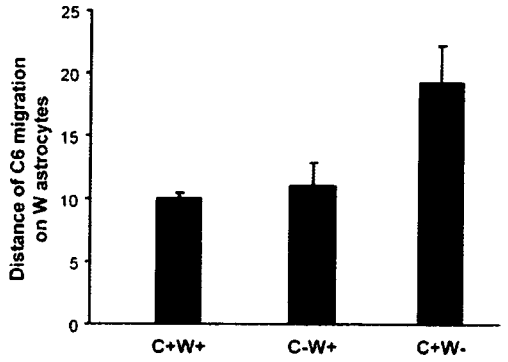

Fig. 3. Migratory capacity of C6 cells on monolayers of white matter astrocytes. Quantitative analysis of the total distances of migratory movements of C6/EGFP cells on white matter astrocytes recorded during a period of 2 h under time-lapse microscopy. Mts1/S100A4 positive (C+) and negative (C−) C6 cells showed a little migratory movements on Mts1/S100A4 expressing white matter astrocytes (W+). In contrast, migratory movements of Mts1/S100A4 positive C6 cells (C+) were markedly increased following silencing of Mts1/S100A4 expression in white matter astrocytes (W−).

EGFP cells showed signs of motility on astrocytes during a period of 2 h. C6/EGFP cells treated with Mts1/S100A4 siRNA (2nd group) displayed changes in their shape on astrocytes, but did not change their position. Interestingly, however, on Mts1/S100A4-silenced white matter astrocytes (3rd group), C6/EGFP cells consistently displayed continuous movements at the cell surface with processes emerging and withdrawing in different directions. These results indicate that the migration of C6 cells, regardless of Mts1/S100A4 expression, is restricted and influenced by the Mts1/S100A4 expression level of the interacting white matter astrocytes.

Transplantation to corpus callosum

We analyzed two types of experiments: (1) C6/EGFP cells positive for Mts1/S100A4 transplanted to corpus callosum (C+W+), and (2) C6/EGFP cells with down-regulated Mts1/S100A4 expression transplanted to corpus callosum (C−W+). Transplantation experiments were terminated on the fourth day after C6 cell injection to avoid a post-grafting up-regulation of Mts1/S100A4 expression after siRNA mediated Mts1/S100A4 silencing. Transverse sections through the brain were examined in the fluorescence microscope and all sections containing EGFP positive cells were collected. Thus, we could estimate the rostro-caudal distribution of C6/EGFP cells in the recipient brains by counting the number of sections containing C6/EGFP cells. The distribution of the C6/EGFP cells in medio-lateral direction was estimated by measuring the distance of C6 cell distribution from the midline in the section series through the entire transplant. We also analyzed the distribution of each transplant with regard to their location in white or gray matter areas. Serial sections were prepared from all transplants and reconstructed for this analysis. Surprisingly, C6/EGFP cells expressing Mts1/S100A4 migrated in the brain in the rostro-caudal direction for shorter distance than C6/EGFP cells after treatment with Mts1/S100A4 siRNA (Fig. 4A). Furthermore, all transplants with C6/EGFP cells expressing Mts1/S100A4 preferentially migrated in corpus callosum (Figs. 4B and 5A) whereas C6/EGFP cells silenced for Mts1/S100A4 avoided white matter and migrated in gray matter along meninges and blood vessels (Figs. 4C and 5B).

Metalloproteinase expression of C6 cells

To investigate whether the difference of the *in vivo* migration pattern between Mts1/S100A4-expressing and -silenced C6 cells could be due to any changes of metalloproteinase activities, we analyzed the expressions of MMP-2, MMP-9, and MT1-MMP, or their inhibitors, TIMP-1 and TIMP-2, at the mRNA level. However, C6 cells did not change their expression of these mRNAs in response to the change of Mts1/S100A4 expression (Fig. 6). Consistent with these results, a zymography analysis showed that C6 cells secreted almost equal amounts of MMP2 and

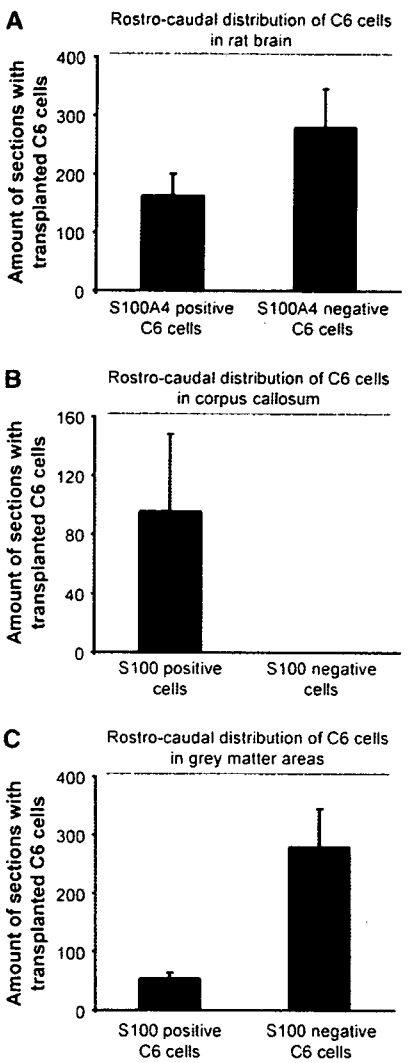

Fig. 4. Data from measurements of rostro-caudal migration of C6/EGFP cells transplanted to the rat brain. Mts1/S100A4 expressing C6 cells migrated for shorter distances in the rostro-caudal direction than C6 cells treated with S100A4siRNA (A). However, all Mts1/S100A4 expressing C6/EGFP cells preferentially migrated in corpus callosum (B), whereas C6/EGFP cells silenced for Mts1/S100A4 preferably migrated in gray matter areas—along meninges and blood vessels (C).

Please cite this article as: Takenaga, K., et al., Modified expression of Mts1/S100A4 protein in C6 glioma cells or surrounding astrocytes affects migration of tumor cells *in vitro* and *in vivo*, Neurobiol. Dis. (2006), doi:10.1016/j.nbd.2006.10.021

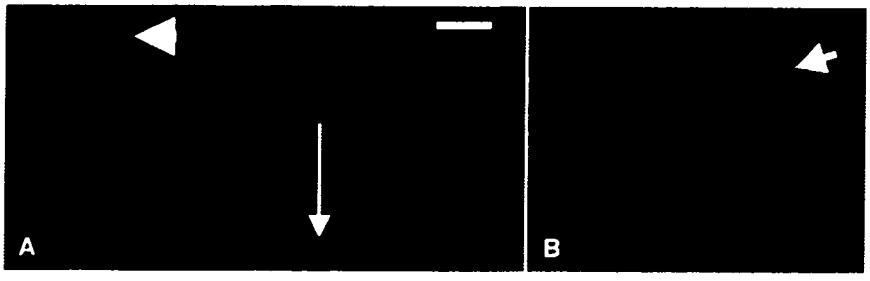

Fig. 5. Coronal sections of C6/EGFP cells transplanted to the adult rat corpus callosum. Migration of transplanted Mts1/S100A4 expressing C6 cells is mainly restricted to corpus callosum (A), whereas C6 cells treated with S100A4 siRNA before transplantation, avoided white matter and preferred to migrate in gray matter (B). Arrowhead (A)=transplant site; arrow (A)=midline; arrow (B)=meningeal surface of the brain. Scale bar=100 μm.

MMP9 irrespective of Mts1/S100A4 expression level (data not shown).

Differential expression of the S100A4/Mts1 gene in astrocytic tumors

To examine whether there is a difference in the expression level of Mts1/S100A4 mRNA in various grades of astrocytic tumors, we carried out real-time quantitative PCR. The results clearly show that the relative Mts1/S100A4 mRNA expression level in glioblastomas (grade 4) was higher than that in pilocytic astrocytomas (grade 1), diffuse astrocytomas (grade 2), and anaplastic astrocytomas (grade 3) (Fig. 7). Although there was no significant difference between diffuse astrocytoma and anaplastic astrocytoma, the difference between glioblastoma and other astrocytomas (pilocytic astrocytoma+diffuse astrocytoma+anaplastic astrocytoma) was statistically significant ($p<0.03$). We conclude that high-grade glioblastomas express higher amount of S100A4/Mts1 than other low-grade astrocytic tumors.

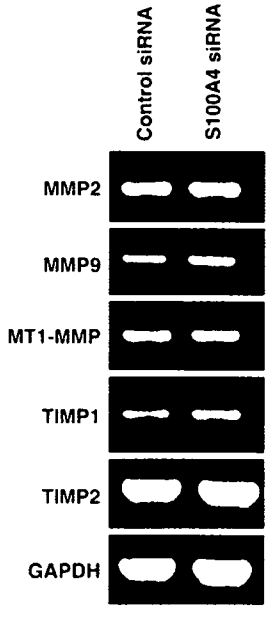

Fig. 6. RT-PCR analysis of the expression of metalloproteinases and their inhibitors in Mts1/S100A4 siRNA-transfected C6 glioma cells. C6 glioma cells were transfected with 100 nM control siRNA or Mts1/S100A4 siRNA. Three days after the transfection, total RNA was prepared using the TRIzol method. After reverse transcription, the resulting cDNAs were applied to PCR using rat MMP-2-, MMP-9-, MT1-MMP-, TIMP-1-, and TIMP-2-specific primer pairs. GAPDH was used as an internal control to estimate the expression levels of the genes. No changes are found in the expression of MMP-2, -9, MT1-MMP, or TIMP1 and 2 in Mts1/S100A4 siRNA-treated C6 glioma cells.

Discussion

Mts1/S100A4 has been strongly implicated in invasion and metastasis of many non-neural tumors (reviewed in Helfman et al., 2005), and is up-regulated also in many brain tumors (Camby et al., 1999; Heman et al., 2003). In our study, we found that high-grade glioblastomas indeed express higher amount of S100A4/Mts1 than other low-grade astrocytic tumors. Together with our *in vitro* experiments and *in vivo* transplantation experiments of C6 glioma cells, we found that the level of Mts1/S100A4 in glioma cells as well as in surrounding astrocytes has a profound influence on the ability of glioma cells to invade the central nervous system.

To elucidate the role of Mts1/S100A4 in C6 cells and astrocytes in their interactions, we analyzed how the morphology and migratory behavior *in vitro* and *in vivo* of Mts1/S100A4 positive or

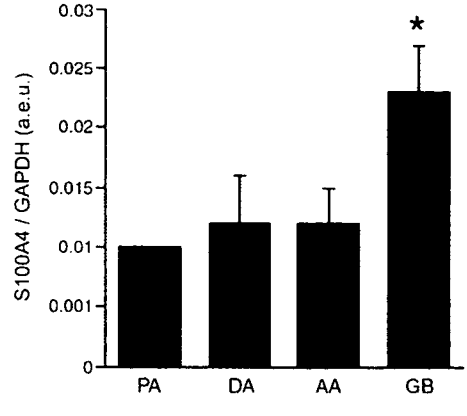

Fig. 7. Quantitative RT-PCR analysis for the expression of Mts1/S100A4 in various grades of astrocytic tumors. PA, DA, AA, and GB indicate pilocytic astrocytomas ($n=1$), diffuse astrocytomas ($n=5$), anaplastic astrocytomas ($n=10$), and glioblastoma ($n=14$), respectively. *Statistically significant between glioblastoma and other astrocytomas ($p<0.03$). Columns, mean; Bars, SE.

Please cite this article as: Takenaga, K., et al., Modified expression of Mts1/S100A4 protein in C6 glioma cells or surrounding astrocytes affects migration of tumor cells *in vitro* and *in vivo*, Neurobiol. Dis. (2006), doi:10.1016/j.nbd.2006.10.021

negative C6 cells are influenced by contact with Mts1/S100A4 positive or negative astrocytes. For this, cultures of astrocytes were prepared from the corpus callosum of P4 old rats (Kozlova and Takenaga, 2005), and Mts1/S100A4 expression in these astrocytes was silenced with siRNA. When C6 cells were seeded on Mts1/S100A4-positive white matter astrocytes, C6 cells remained round, irrespective of whether they expressed Mts1/S100A4 or not. However, the majority of C6 cells displayed a flat shape on Mts1/S100A4-silenced white matter astrocytes. These findings show that the properties of neighboring astrocytes are the major determinants in influencing the shape of C6 cells *in vitro*, and that Mts1/S100A4-negative astrocytes promote the emergence of a flat C6 cell shape.

We postulated that the change in cell shape from round to flat provides an indicator of potential cell motility, although actual migration may require additional stimuli. To corroborate this, we recorded the migration of C6 cells in time-lapse microscopy assay and found that Mts1/S100A4-silenced astrocytes promote the migration of C6 glioma cells. We previously showed that siRNA mediated down-regulation of Mts1/S100A4 in white matter astrocytes *in vitro* increases their motility, changes the organization of their actin cytoskeleton, and increases their expression and activity of MMP-9 and MT1-MMP (23). These changes may contribute to the ability of Mts1/S100A4-silenced white matter astrocytes to promote C6 cell migration. Alternatively, astrocyte Mts1/S100A4 may promote astrocyte–C6 cell interactions via one of its targets, liprin β1, thereby influencing the LAR-liprin α1-liprin β1 network, which regulates cytoskeletal dynamics and cell adhesion (Kriajevska et al., 2002). It is also possible that extracellular Mts1/S100A4 released from white matter astrocytes regulates C6 cell migration, because it has been reported that extracellular Mts1/S100A4 affects a variety of biological events including bone mineralization (Duarte et al., 1999; Kato et al., 2005), cell motility (Belot et al., 2002), tumor-stroma interplay (Schmidt-Hansen et al., 2004a,b), neurite outgrowth (Novitskaya et al., 2000; Fang et al., 2006), and intracellular S100 protein translocations (Hsieh et al., 2004).

A common, although still controversial notion is that white matter is non-permissive to neurite growth and cell migration due to its presence of oligodendrocytes and myelin (Bandtlow and Schwab, 2000; McGee and Strittmatter, 2003; Raisman, 2004). Previously we have shown that that white but not gray matter astrocytes expressed Mts1/S100A4 protein *in vivo* (Kozlova and Lukanidin, 1999; Åberg and Kozlova, 2000). To explore the possible role of intracellular Mts1/S100A4 in C6 cells, we compared the migration of Mts1/S100A4-expressing and -silenced C6 cells after transplantation to corpus callosum. Although both types of C6 cells demonstrated strong capacity to migrate in the adult brain, there were marked differences in the distribution of Mts1/S100A4-expressing and -silenced C6 cells. Mts1/S100A4-expressing C6 cells migrated preferentially in corpus callosum where Mts1/S100A4 is strongly expressed, whereas Mts1/S100A4-silenced C6 cells avoided white matter areas but displayed strong motility in gray matter areas where Mts1/S100A4 are negative. These results suggest that interactions between white matter astrocytes and Mts1/S100A4-expressing C6 cells which tend to maintain these C6 cells in white matter no longer operate in Mts1/S100A4-silenced C6 cells. As a result, C6 cells become less restricted to white matter.

The underlying molecular mechanisms of the *in vivo* behavior of Mts1/S100A4-expressing and -silenced C6 cells are presently obscure. It has been shown that the expression of MT1-MMP on the surface of the C6 cell was associated with a remodeling of the non-permissive CNS myelin substrate into a permissive one, thereby allowing spreading, migration, and infiltration of glioma cells (Belien et al., 1999). We previously demonstrated that intracellular Mts1/S100A4 influences the expression levels of MMP-9 and MT1-MMP in white matter astrocytes (Takenaga and Kozlova, 2006). Therefore, one possible mechanism was the changes of metalloproteinase activities in C6 cells. However, our data did not support this mechanism. Another possible mechanism could be the influence of Mts1/S100A4 on transcription of some particular genes regulating morphology, motility, or adhesion properties of tumor cells. Indeed, we have demonstrated that Mts1/S100A4 can modulate the expression of several p53-regulated genes. The effect of Mts1/S100A4 on cellular properties was dependent on the particular genes and cellular environment (Grigorian et al., 2001). This implicates that down-regulation of intracellular Mts1/S100A4 certainly may modify expression of some genes in C6 glioma cells which could affect C6 cell migration itself as well as C6 cell-astrocyte interactions *in vivo*. Elucidation of such genes may provide us some clues for understanding the *in vivo* invasion pattern of C6 tumor cells.

Our data implicate Mts1/S100A4 in migration of C6 glioma cells *in vitro* as well as *in vivo*, and emphasizes the possible significance of the properties of the cellular environment with which glioma cells interact. Importantly, intracellular Mts1/S100A4 expression promotes migration of C6 glioma cells in white matter areas, whereas silencing of Mts1/S100A4 induces migration of C6 cells on blood vessels and meninges. An extension of this proposal would be that low grade gliomas, which do not express Mts1/S100A4, preferentially migrate along meninges and blood vessels, whereas Mts1/S100A4 positive malignant gliomas tend to spread in white matter areas. Mts1/S100A4 may therefore be an important factor in the pathogenesis of highly malignant brain tumors.

Acknowledgments

Grant Support: The Swedish Science Council, proj. 5420. Grant-in-Aid from the Ministry of Health, Labour, and Welfare for Third Term Comprehensive Control Research for Cancer and from the Ministry of Education, Culture, Sports, Science and Technology, Japan. KT was supported by a visiting scientist fellowship from the Swedish Foundation for International Cooperation in Science and Education. EL was supported by Danish Cancer Society and a European Union BRECOSM-LSH-CT 503234 FP6 grant. We are grateful to Ms. Britta Isaksson for expert assistance with the stereotaxical transplantations and to Mss. Nadja Duthoit and Naomi Forslund for assistance with the cultures.

References

Åberg, F., Kozlova, E.N., 2000. Metastasis-associated Mts1 (S100A4) protein in the developing and adult central nervous system. J. Comp. Neurol. 424, 269–282.

Amberger, V.R., Paganetti, P.A., Seulberger, H., Eldering, J.A., Schwab, M.E., 1994. Characterization of a membrane-bound metalloendoprotease of rat C6 glioblastoma cells. Cancer Res. 54, 4017–4025.

Amberger, V.R., Hensel, T., Ogata, N., Schwab, M.E., 1998. Spreading and migration of human glioma and rat C6 cells on central nervous system myelin in vitro is correlated with tumor malignancy and involves a metalloproteolytic activity. Cancer Res. 58, 149–158.

Please cite this article as: Takenaga, K., et al., Modified expression of Mts1/S100A4 protein in C6 glioma cells or surrounding astrocytes affects migration of tumor cells *in vitro* and *in vivo*, Neurobiol. Dis. (2006), doi:10.1016/j.nbd.2006.10.021

Bandtlow, C., Schwab, M., 2000. NI-35/250/nogo-a: a neurite growth inhibitor restricting structural plasticity and regeneration of nerve fibers in the adult vertebrate CNS. Glia 29, 175–181.

Belien, A.T., Paganetti, P.A., Schwab, M.E., 1999. Membrane-type 1 matrix metalloprotease (MT1-MMP) enables invasive migration of glioma cells in central nervous system white matter. J. Cell Biol. 144, 373–384.

Belot, N., Pochet, R., Heizmann, C.W., Kiss, R., Decaestecker, C., 2002. Extracellular S100A4 stimulates the migration rate of astrocytic tumor cells by modifying the organization of their cytoskeleton. Biochim. Biophys. Acta 1600, 74–83.

Benda, P., Lightbody, J., Sato, G., Levine, L., Sweet, W., 1968. Differentiated rat glial cell strain in tissue culture. Science 161, 370–371.

Camby, I., Nagy, N., Lopes, M.B., Schafer, B.W., Maurage, C.A., Ruchoux, M.M., Murmann, P., Pochet, R., Heizmann, C.W., Brotchi, J., Salmon, I., Kiss, R., Decaestecker, C., 1999. Supratentorial pilocytic astrocytomas, astrocytomas, anaplastic astrocytomas and glioblastomas are characterized by a differential expression of S100 proteins. Brain Pathol. 9, 1–19.

Chomczynski, P., Sacchi, N., 1987. Single-step method of RNA isolation by acid guanidinium thiocyanate–phenol–chloroform extraction. Anal. Biochem. 162, 156–159.

Duarte, W.R., Iimura, T., Takenaga, K., Ohya, K., Ishikawa, I., Kasugai, S., 1999. Extracellular role of S100A4 calcium-binding protein in the periodontal ligament. Biochem. Biophys. Res. Commun. 255, 416–420.

Fang, Z., Forslund, N., Takenaga, K., Lukanidin, E., Kozlova, E.N., 2006. Sensory neurite outgrowth on white matter astrocytes is influenced by intracellular and extracellular S100A4 protein. J. Neurosci. Res. 83, 619–626.

Giese, A., Kluwe, L., Laube, B., Meissner, H., Berens, M.E., Westphal, M., 1996. Migration of human glioma cells on myelin. Neurosurgery 38, 755–764.

Grigorian, M., Andresen, S., Tulchinsky, E., Kriajevska, M., Carlberg, C., Kruse, C., Cohn, M., Ambartsumian, N., Christensen, A., Selivanova, G., Lukanidin, E., 2001. Tumor suppressor p53 protein is a new target for the metastasis-associated Mts1/S100A4 protein: functional consequences of their interaction. J. Biol. Chem. 276, 22699–22708.

Guillamo, J.S., Lisovoski, F., Christov, C., Le Guerinel, C., Defer, G.L., Peschanski, M., Lefrancois, T., 2001. Migration pathways of human glioblastoma cells xenografted into the immunosuppressed rat brain. J. Neuro-Oncol. 52, 205–215.

Helfman, D.M., Kim, E.J., Lukanidin, E., Grigorian, M., 2005. The metastasis associated protein S100A4: role in tumour progression and metastasis. Br. J. Cancer 92, 1955–1958.

Hensel, T., Amberger, V.R., Schwab, M.E., 1998. A metalloprotease activity from C6 glioma cells inactivates the myelin-associated neurite growth inhibitors and can be neutralized by antibodies. Br. J. Cancer 78, 1564–1572.

Herman, R., Fasheh, R., Calabrese, C., Frank, A.J., Maclean, K.H., Allard, D., Barraclough, R., Gilbertson, R.J., 2003. ERBB2 up-regulates S100A4 and several other prometastatic genes in medulloblastoma. Cancer Res. 63, 140–148.

Hormigo, A., McCarthy, M., Nothias, J.M., Hasegawa, K., Huang, W., Friedlander, D.R., Fischer, I., Fishell, G., Grumet, M., 2001. Radial glial cell line C6-R integrates preferentially in adult white matter and facilitates migration of coimplanted neurons in vivo. Exp. Neurol. 168, 310–322.

Hsieh, H.L., Schafer, B.W., Weigle, B., Heizmann, C.W., 2004. S100 protein translocation in response to extracellular S100 is mediated by in human endothelial cells. Biochem Biophys. Res. Commun. 316, 949–959.

Kato, C., Kojima, T., Komaki, M., Mimori, K., Duarte, W.R., Takenaga, K., Ishikawa, I., 2005. S100A4 inhibition by RNAi up-regulates osteoblast related genes in periodontal ligament cells. Biochem. Biophys. Res. Commun. 326, 147–153.

Kleihues, P., Cavanee, W.K., 1997. Pathology and Genetics of Tumours of the Nervous System. International Agency for Research on Cancer (IARC), Lyon, France, pp. 49–55.

Kozlova, E.N., Lukanidin, E., 1999. Metastasis-associated Mts1 (S100A4) protein is selectively expressed in white matter astrocytes and is up-regulated after peripheral nerve or dorsal root injury. Glia 27, 249–258.

Kozlova, E.N., Lukanidin, E., 2002. Mts1 protein expression in the central nervous system after injury. Glia 37, 337–348.

Kozlova, E.N., Takenaga, K., 2005. A procedure for culturing astrocytes from white matter and the application of the siRNA technique for silencing the expression of their specific marker, S100A4. Brain Res. Brain Res. Protoc. 15, 59–65.

Kriajevska, M., Fischer-Larsen, M., Moertz, E., Vorm, O., Tulchinsky, E., Grigorian, M., Ambartsumian, N., Lukanidin, E., 2002. Liprin beta 1, a member of the family of LAR transmembrane tyrosine phosphatase-interacting proteins, is a new target for the metastasis-associated protein S100A4 (Mts1). J. Biol. Chem. 277, 5229–5235.

Lefranc, F., Brotchi, J., Kiss, R., 2005. Possible future issues in the treatment of glioblastomas: special emphasis on cell migration and the resistance of migrating glioblastoma cells to apoptosis. J. Clin. Oncol. 23, 2411–2422.

McGee, A.W., Strittmatter, S.M., 2003. The Nogo-66 receptor: focusing myelin inhibition of axon regeneration. Trends Neurosci. 26, 193–198.

Namba, H., Tagawa, M., Miyagawa, T., Iwadate, Y., Sakiyama, S., 2000. Treatment of rat experimental brain tumors by herpes simplex virus thymidine kinase gene-transduced allogeneic tumor cells and ganciclovir. Cancer Gene Ther. 7, 947–953.

Novitskaya, V., Grigorian, M., Kriajevska, M., Tarabykina, S., Bronstein, I., Berezin, V., Bock, E., Lukanidin, E., 2000. Oligomeric forms of the metastasis-related Mts1 (S100A4) protein stimulate neuronal differentiation in cultures of rat hippocampal neurons. J. Biol. Chem. 275, 41278–41286.

Paganetti, P.A., Caroni, P., Schwab, M.E., 1988. Glioblastoma infiltration into central nervous system tissue in vitro: involvement of a metalloprotease. J. Cell Biol. 107, 2281–2291.

Pedersen, P.H., Edvardsen, K., Garcia-Cabrera, I., Mahesparan, R., Thorsen, J., Mathisen, B., Rosenblum, M.L., Bjerkvig, R., 1995. Migratory patterns of lac-z transfected human glioma cells in the rat brain. Int. J. Cancer 62, 767–771.

Raisman, G., 2004. Myelin inhibitors: does NO mean GO? Nat. Rev., Neurosci. 5, 157–161.

Schmidt-Hansen, B., Klingelhofer, J., Grum-Schwensen, B., Christensen, A., Andresen, S., Kruse, C., Hansen, T., Ambartsumian, N., Lukanidin, E., Grigorian, M., 2004a. Functional significance of metastasis-inducing S100A4 (Mts1) in tumor-stroma interplay. J. Biol. Chem. 279, 24498–24504.

Schmidt-Hansen, B., Ornas, D., Grigorian, M., Klingelhofer, J., Tulchinsky, E., Lukanidin, E., Ambartsumian, N., 2004b. Extracellular S100A4 (mts1) stimulates invasive growth of mouse endothelial cells and modulates MMP-13 matrix metalloproteinase activity. Oncogene 23, 5487–5495.

Schwab, M.E., Caroni, P., 1988. Oligodendrocytes and CNS myelin are nonpermissive substrates for neurite growth and fibroblast spreading in vitro. J. Neurosci. 8, 2381–2393.

Spillmann, A.A., Amberger, V.R., Schwab, M.E., 1997. High molecular weight protein of human central nervous system myelin inhibits neurite outgrowth: an effect which can be neutralized by the monoclonal antibody IN-1. Eur. J. Neurosci. 9, 549–555.

Takenaga, K., Kozlova, E.N., 2006. Role of intracellular S100A4 for migration of rat astrocytes. Glia 53, 313–321.

Takenaga, K., Nakamura, Y., Sakiyama, S., 1994. Cellular localization of pEL98 protein, an S100-related calcium binding protein, in fibroblasts and its tissue distribution analyzed by monoclonal antibodies. Cell Struct. Funct. 19, 133–141.

Please cite this article as: Takenaga, K., et al., Modified expression of Mts1/S100A4 protein in C6 glioma cells or surrounding astrocytes affects migration of tumor cells *in vitro* and *in vivo*, Neurobiol. Dis. (2006), doi:10.1016/j.nbd.2006.10.021

Oncogene (2007), 1–9

www.nature.com/onc

ORIGINAL ARTICLE

Novel risk stratification of patients with neuroblastoma by genomic signature, which is independent of molecular signature

N Tomioka[1,2,3,11], S Oba[4,11], M Ohira[1,11], A Misra[2,12], J Fridlyand[5], S Ishii[4,13], Y Nakamura[1], E Isogai[1], T Hirata[6], Y Yoshida[7], S Todo[3], Y Kaneko[8], DG Albertson[9,10], D Pinkel[9,10], BG Feuerstein[2,9,10,12] and A Nakagawara[1]

[1]*Division of Biochemistry, Chiba Cancer Center Research Institute, Chiba, Japan;* [2]*Department of Neurological Surgery, Brain Tumor Research Center, University of California, San Francisco, CA, USA;* [3]*Department of Surgery, Hokkaido University School of Medicine, Sapporo, Japan;* [4]*Graduate School of Information Science, Nara Institute of Science and Technology, Ikoma, Japan;* [5]*Department of Epidemiology and Biostatistics, University of California, San Francisco, CA, USA;* [6]*Hisamitsu Pharmaceutical Co. Inc., Tokyo, Japan;* [7]*GENESHOT project, R&D Center, NGK Insulators, Ltd, Nagoya, Japan;* [8]*Saitama Cancer Center Research Institute, Saitama, Japan;* [9]*Department of Laboratory Medicine, University of California, San Francisco, CA, USA and* [10]*Comprehensive Cancer Center, University of California, San Francisco, CA, USA*

Human neuroblastoma remains enigmatic because it often shows spontaneous regression and aggressive growth. The prognosis of advanced stage of sporadic neuroblastomas is still poor. Here, we investigated whether genomic and molecular signatures could categorize new therapeutic risk groups in primary neuroblastomas. We conducted microarray-based comparative genomic hybridization (array-CGH) with a DNA chip carrying 2464 BAC clones to examine genomic aberrations of 236 neuroblastomas and used in-house cDNA microarrays for gene-expression profiling. Array-CGH demonstrated three major genomic groups of chromosomal aberrations: silent (GGS), partial gains and/or losses (GGP) and whole gains and/or losses (GGW), which well corresponded with the patterns of chromosome 17 abnormalities. They were further classified into subgroups with different outcomes. In 112 sporadic neuroblastomas, *MYCN* amplification was frequent in GGS (22%) and GGP (53%) and caused serious outcomes in patients. Sporadic tumors with a single copy of *MYCN* showed the 5-year cumulative survival rates of 89% in GGS, 53% in GGP and 85% in GGW. Molecular signatures also segregated patients into the favorable and unfavorable prognosis groups ($P=0.001$). Both univariate and multivariate analyses revealed that genomic and molecular signatures were mutually independent, powerful prognostic indicators. Thus, combined genomic and molecular signatures may categorize novel risk groups and confer new clues for allowing tailored or even individualized medicine to patients with neuroblastoma.

Oncogene advance online publication, 16 July 2007; doi:10.1038/sj.onc.1210661

Keywords: neuroblastoma; array-CGH; molecular signature; risk stratification; microarray

Introduction

Neuroblastoma is one of the most common solid tumors in children. However, its clinical behavior is enigmatic because the tumor usually regresses spontaneously when developed in patients under 1 year of age, but often grows rapidly to cause fatal outcomes when developed as an advanced tumor in patients over the age of 1 year (Brodeur, 2003; Schwab *et al.*, 2003). Recent nationwide mass screening (MS) in Japan for discovering neuroblastoma at the age of 6 months clearly demonstrated the presence of a large number of asymptomatic tumors undergoing spontaneous regression (Woods *et al.*, 2002), which had been suggested by Beckwith and Perrin (1963). The involvement of TrkA, a high-affinity receptor for nerve growth factor, in the regression of neuroblastoma has been suggested; however, the molecular mechanisms of the regressive event still remain elusive (Nakagawara *et al.*, 1993; Nakagawara, 1998). On the other hand, the majority of sporadic neuroblastomas are discovered at advanced stages, and their prognosis is still very poor (Brodeur, 2003; Schwab *et al.*, 2003). Recently advanced cytogenetic analyses revealed that given subsets of neuroblastomas with a favorable prognosis possess the hyperdiploid karyotype of chromosomes (Look *et al.*, 1984; Tomioka *et al.*, 2003) and that the other subsets with an unfavorable prognosis usually possess the diploid or tetraploid karyotype and often have *MYCN* amplification, gains of chromosome arms 1q, 2p and 17q, as well as allelic losses of chromosome arms 1p, 3p and 11q (Brodeur,

Correspondence: Dr A Nakagawara, Division of Biochemistry, Chiba Cancer Center Research Institute, 666-2 Nitona, Chuoh-Ku, Chiba 260-8717, Japan.
E-mail: akiranak@chiba-cc.jp
[11]These authors contributed equally to this work.
[12]Current address: Department of Neurology, Barrow Neurological Institute, St. Joseph's Hospital and Medical Center, Phoenix, AZ, USA.
[13]Current address: Graduate School of Informatics, Kyoto University, Kyoto, Japan.
Received 29 December 2006; revised 29 May 2007; accepted 11 June 2007

2003; Schwab *et al*., 2003). We and other investigators have previously reported the high accuracy of gene-expression profiling to predict the prognosis of neuroblastoma (Wei *et al*., 2004; Ohira *et al*., 2005). However, the prognostic significance of genomic signatures when using a high-resolution DNA microarray in primary neuroblastomas has never been reported. Here, we applied microarray-based comparative genomic hybridization (array-CGH) to both sporadic and MS-detected neuroblastomas in order to comprehend their clinical behavior and found that genomic signatures, together with molecular signatures, stratified the novel risk groups in sporadic neuroblastomas.

Results

Patterns of genomic signatures in 236 primary neuroblastomas

The most prominent feature of 236 primary neuroblastomas (112 sporadic and 124 MS detected) was the apparent presence of three genomic groups (GGs) (Figure 1a, its magnified, high-resolution figures are also indicated in Supplementary Figures S1a and b): the group of few chromosomal events (silent, GGS; $n=29$); the group of partial chromosomal gains/losses (GGP; $n=77$) and the group of whole chromosomal gains/losses (GGW; $n=130$) (Supplementary Figures S2a and b). Correlation analysis revealed that the global feature (see Materials and methods) was maximally correlated with the gain of the long arm of chromosome 17 ($R=-0.807$) and with the gain of a whole chromosome 17 ($R=0.75$) (Supplementary Table S1a), therefore the genomic groups GGP and GGW were defined by the status of aberration, by 17q gain and 17 whole chromosomal gain occurred in chromosome 17, respectively. They were followed by DNA ploidy ($R=-0.642$), loss of chromosome 1p ($R=-0.521$), *MYCN* amplification ($R=-0.531$), loss of chromosome 11q ($R=-0.5$), low *TrkA* expression ($R=-0.47$) and age$\geqslant$1-year old ($R=-0.466$). Even when tested in 112 sporadic tumors, the correlation coefficient was -0.773 in 17q gain, -0.705 in DNA ploidy, -0.598 in 1p loss, -0.565 in tumor stages, -0.502 in *MYCN* amplification, -0.49 in low *TrkA* expression and -0.458 in age$\geqslant$1-year old (Supplementary Table S1b). These suggested that 17q gain was a characteristic and prognosis-related event in primary neuroblastomas. The percentages of DNA diploidy or tetraploidy were 83% (15/18), 66% (33/50) and 18% (17/94) in GGS, GGP and GGW tumors, respectively (Supplementary Table S2a).

GGS tumors rarely showed chromosomal aberrations except *MYCN* amplification in 5 among 29 tumors (Figure 1b, a high-resolution figure is also indicated in Supplementary Figure S1c). To date, the presence of the GGS subgroup with very silent aberrations of the tumor genome has never been verified definitely. The concern about the possible dilution of the tumor-cell DNA content by contamination of stromal cells was cleared by the detailed examination of GGS tumor specimens (see Supplementary Figure S2b and Supplementary Information).

Seventy-seven GGP tumors, which had 17q gain, were further subgrouped computationally according to the detailed chromosomal event, the presence and/or absence of 1p loss and 11q loss, which are characteristic and *MYCN* amplification (s, single copy of *MYCN*; a, *MYCN* amplification) (Figures 1a and b, and see Supplementary Information). GGP1 tumors were characterized by 1p loss and 17q gain as main aberrations. GGP1a ($n=23$) was one of the most common GGP tumors. They showed the diploid karyotype (10/13, 77%) and had *MYCN* amplification in addition to 1p loss and 17q gain. Interestingly, GGP1s tumors lacking *MYCN* amplification ($n=6$) showed relatively frequent 2p gain, as well as 14q loss, 1q gain, 4p loss and 7p gain that were rare in GGP1a tumors with *MYCN* amplification. GGP2 tumors were characterized by the presence of both 1p loss and 11q loss, in addition to 17q gain. In GGP2a, tumors with *MYCN* amplification ($n=4$) also frequently showed 1q gain. GGP3 tumors formed a group typically characterized by the presence of 11q loss and 17q gain without 1p loss. Intriguingly, only 1 of 27 GGP3 tumors had *MYCN* amplification. All GGP4 tumors except one, which presented neither 1p loss nor 11q loss, also had no *MYCN* amplification. The percentages of diploidy/tetraploidy in GGP1, GGP2, GGP3 and GGP4 tumors were 76% (13/17), 75% (6/8), 76% (13/17) and 13% (1/8), respectively (Supplementary Table S2a).

GGW tumors with whole chromosomal gains and/or losses, especially with the predominant gain of whole chromosome 17 (Figure 1b), were mostly the tumors detected by MS (94/130, 73%; see Supplementary Table S2a). The highest incidence of MS-detected neuroblastomas was observed in GGW4s tumors that were purely composed of whole chromosomal gains/losses. The DNA ploidy analysis revealed that 82% (77/94) of GGW tumors were hyperdiploidy. Similarly to GGP tumors, GGW tumors were categorized into tumors with the following aberrations: 1p loss (GGW1, $n=5$); both 1p loss and 11q loss (GGW2, $n=2$); 11q loss (GGW3, $n=11$) and without any one (GGW4, $n=92$). GGW5 tumors ($n=20$) formed a group of tumors with a low frequency of chromosome 17 on the BAC array. Like chromosome 17, chromosomes 6 and 7 were frequently gained in GGW tumors. *MYCN* amplification was observed in only three tumors belonging to GGW4 or GGW5 (3/112, 2.7%).

Genomic signatures and clinical outcomes

Genomic signatures of neuroblastomas unveiled previously unknown relationships between genetic subgroup and patient prognosis (Figure 1b). The greatest surprise was the difference in the 5-year survival rates between the GGSa (0%, $n=5$) and GGSs (91%, $n=24$) subgroups ($P<0.001$). The other *MYCN*-amplified tumor subgroups, GGP1a ($n=23$), GGP2a ($n=4$) and GGWa ($n=3$), also showed very poor survival rates of 42, 0 and 0%, respectively. On the other hand, GGWs

neuroblastomas demonstrated good outcomes (GGW1s: 100%, $n=5$; GGW2s: 100%, $n=2$; GGW3s: 100%, $n=11$; GGW4s: 97%, $n=91$ and GGW5s: 89%, $n=18$). The intermediate 5-year cumulative survival rates were demonstrated in GGPs tumors (GGP1s: 80%, $n=6$; GGP2s: 57%, $n=7$; GGP3s: 75%, $n=26$

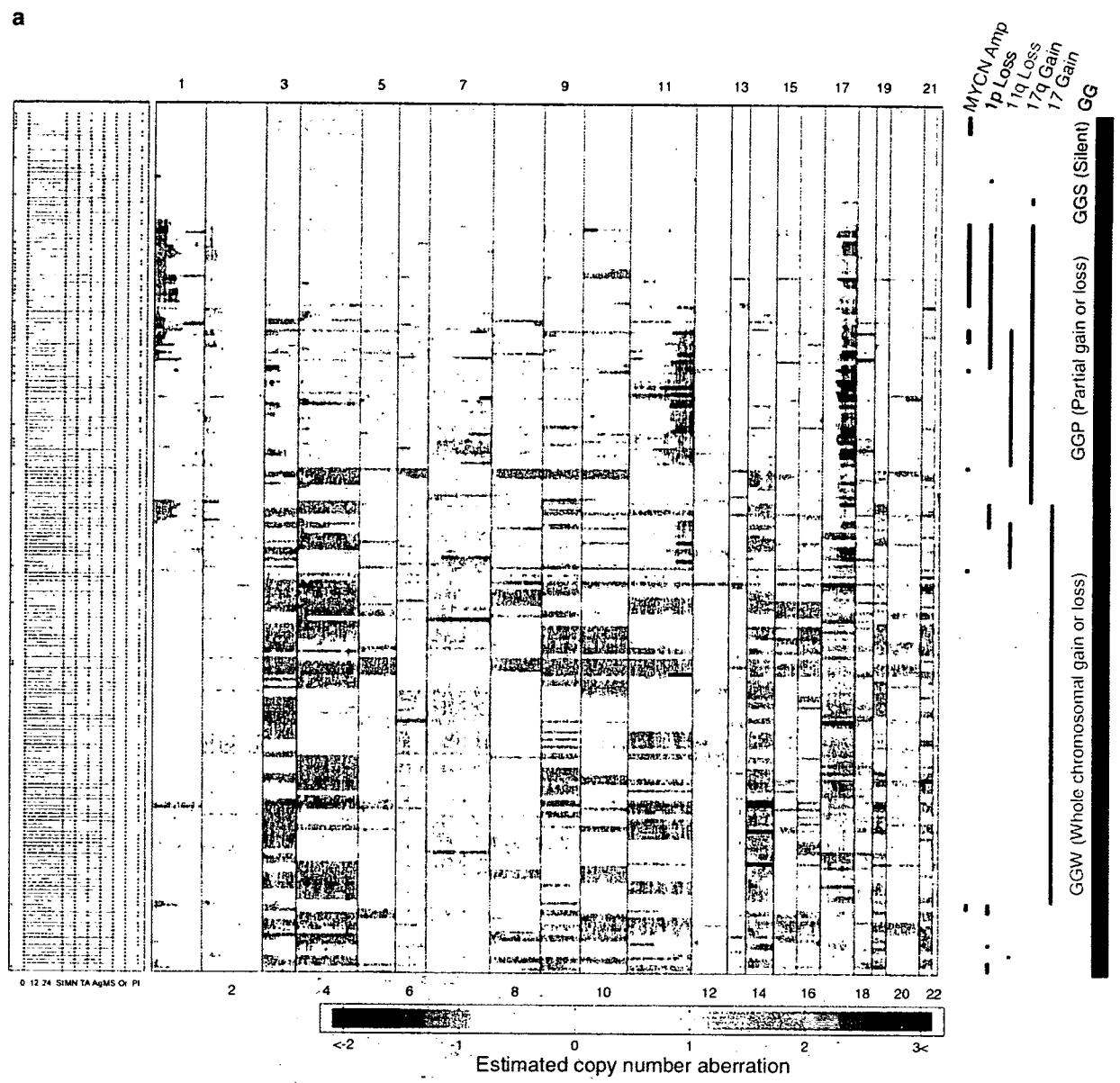

Figure 1 Genomic signatures of 236 primary neuroblastomas by array-based comparative genomic hybridization (array-CGH). **(a)** Overall schematic of the genomic signatures of 236 primary neuroblastomas. The left panel summarizes information about patient diagnostic factors: survival time in months after diagnosis for censored (blue bars) or dead (red bars) patients, stages 1, 2 and 4 s (blue) or 3 and 4 (red) (ST), *MYCN* amplification (red) or not (blue) (MN), TrkA low (red) or high expression (blue) (TA), age more (red) or less (blue) than 12 months (Ag), sporadic tumors (red) or tumors detected by mass screening (blue) (Ms), adrenal gland (red) or others (blue) in origin (Or) and hyperploidy (blue) or diploidy/tetraploidy (red) (Pl). The central panel shows estimated copy number aberrations of DNA as color matrixes (blue: loss, red: gain) at chromosome locations complementary to BAC clones in each sample. The right panel shows the important features of chromosomal events, including *MYCN* amplification, deletions of chromosomes 1p and 11q, chromosome 17q gain and whole chromosome 17 gain. Furthermore, genomic groups (GGS, silent genomic group; GGP, partial chromosomal gains/losses genomic group and GGW, whole gains and/or losses genomic group) are also indicated. **(b)** Genomic signatures in each genomic group and the 5-year survival rates for all neuroblastomas including MS detected and sporadic tumors. Regarding each genomic group, the colored histogram represents the rates of gains and losses for each clone, where the red areas on the baseline correspond to gain and the blue areas under the baseline to loss. The right panel indicates the presence of *MYCN* amplification, 1p loss, 11q loss, 17q gain and 17 gain. The 5-year survival rates (SR) of each genomic subgroup are indicated in the right panel.

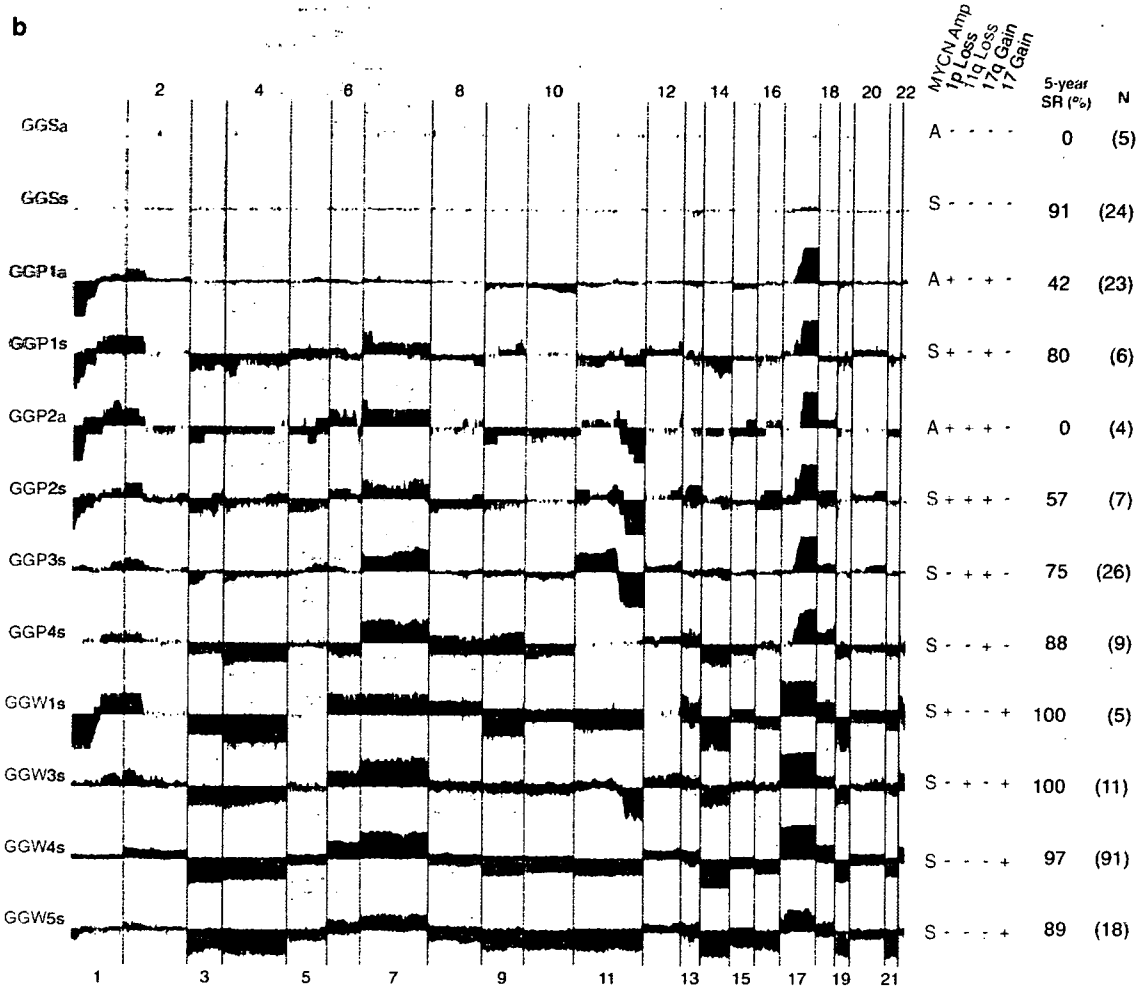

Figure 1 Continued.

and GGP4s: 88%, $n=9$). Interestingly, in GGPs tumors, 1p loss (GGP1s, $n=6$) and 11q loss (GGP3s, $n=26$) seemed to have a similar effect on patient prognosis (5-year survival rates: 80 and 75%, respectively). However, GGP2s tumors with both 1p loss and 11q loss ($n=7$) had a poorer prognosis (57%) in an additive manner. Furthermore, the addition of 11q loss and 1q gain to *MYCN* amplification apparently afforded absolutely poor outcomes as suggested by the comparison between GGP1a (42%) and GGP2a tumors (0%). An analysis of 112 sporadic tumors also revealed a similar tendency except GGP1s, in which 2 sporadic tumors showed 0% survival, whereas all 4 MS-detected tumors gave good outcomes (Table 1 and Supplementary Figure S3). These suggested that *MYCN* amplification had the most powerful influence on clinical outcomes. We next compared the patterns of whole genome abnormalities of *MYCN*-amplified neuroblastomas between survivors (disease-free for more than 2 years after initiating treatment) and non-survivors (dead of disease). One of the most striking differences was frequent loss of 11q (Supplementary Figure S4).

Effects of genomic signatures, MYCN amplification and age on prognosis in sporadic neuroblastomas

Figure 2 shows the Kaplan–Meier cumulative survival curves in each genetic group. In sporadic neuroblastomas, the overall survival rates of GGW, GGS and GGP were 80% ($n=36$), 68% ($n=23$) and 43% ($n=53$), respectively (Figure 2a). The prognosis of GGP was significantly poorer than that of GGW ($P=0.002$). In MS-detected tumors, on the other hand, the survival rates of GGW, GGS and GGP were 100% ($n=94$), 100% ($n=6$) and 96% ($n=24$), respectively (no significant difference among the groups; Figure 2b). The main difference between sporadic and MS-detected tumors was that the latter was detected before 1 year of age and had very few *MYCN* amplifications. Therefore, sporadic tumors were next subcategorized according

to the presence or absence of *MYCN* amplification. Figure 3a shows that the 5-year survival rates of patients with GGSs ($n=18$), GGWs ($n=33$) and GGPs ($n=25$) tumors were 89, 85 and 53%, respectively, whereas those of patients with GGSa ($n-5$), GGWa ($n-3$) and GGPa ($n=28$) tumors involving *MYCN* amplification were 0, 33 and 34%, respectively (Figure 3b). We then further examined the survival curves of patients with *MYCN*-nonamplified tumors in young (<1-year-old) and old (≥1-year-old) patients. Figure 3c shows the 5-year survival rates of 88, 86 and 67% in GGWs ($n=24$), GGSs ($n-7$) and GGPs ($n-3$) tumors, respectively, among young patients, whereas they were 76, 91 and 51% in GGWs ($n=9$), GGSs ($n=11$) and GGPs ($n=22$) tumors, respectively, among old patients (Figure 3d). The former pattern was similar to that in MS-detected tumors, which had high percentages of GGW tumors, whereas the latter contained high incidences of GGP tumors.

Table 1 Five-year overall survival rates of the patients with each genomic subgroup of sporadic neuroblastomas

	N	5-Year OS (%)
GGS		
GGSa	5	0
GGSs	18	89
GGP		
GGP1a	22	44
GGP1s	2	0
GGP2a	4	0
GGP2s	5	40
GGP3a	1	0
GGP3s	15	59
GGP4a	1	0
GGP4s	3	67
GGW		
GGW1a	0	
GGW1s	0	
GGW2a	0	
GGW2s	1	100
GGW3a	0	
GGW3s	3	100
GGW4a	1	0
GGW4s	23	87
GGW5a	2	50
GGW5s	6	67

Abbreviations: GGP, partial chromosomal gains/losses genomic group; GGS, silent genomic group; GGW, whole gains and/or losses genomic group; OS, overall survival rate.

Segregation of the prognosis of sporadic neuroblastomas with a single copy of MYCN by genomic and molecular signatures

Recently, we have generated a clinically useful cDNA microarray carrying 200 genes that predicts the prognosis of neuroblastomas with an accuracy rate of 89% (Ohira *et al*., 2005). The univariate analysis of 112 sporadic neuroblastomas showed that both genomic signatures (GGP vs GGW + GGS, $P=0.003$) and molecular signatures (posterior value<0.5 vs ≥0.5, $P<0.001$) were highly significant prognostic indicators, like other variables including age ($P=0.006$), stage ($P<0.001$), tumor origin ($P=0.001$), *TrkA* expression ($P=0.004$), Shimada classification ($P<0.001$) and *MYCN* amplification ($P<0.001$; Table 2). In addition, genomic signature was a prognostic factor independent from molecular signature, age and tumor origin, although it showed no prognostic significance when stage, Shimada classification, or *MYCN* amplification was controlled (Table 2). Even in sporadic neuroblastomas with a single copy of *MYCN*, the highest significance according to the univariate analysis was given to molecular signature ($P=0.002$), followed by tumor origin ($P=0.006$) and genomic signature ($P-0.010$; Table 2). The multivariate analysis also showed that genomic signature was a prognostic indicator independent from molecular signature or tumor origin (Table 2). As shown in Figure 4, our in-house expression microarrays segregated the survival curves of patients with sporadic tumors lacking *MYCN* amplification (GGSs + GGPs + GGWs) into the favorable (94%, $n-17$) and unfavorable (42%, $n-13$) prognosis groups ($P=0.001$).

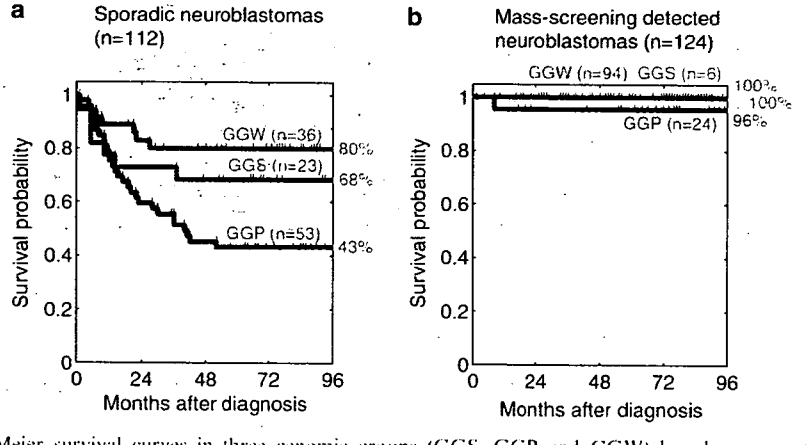

Figure 2 Kaplan Meier survival curves in three genomic groups (GGS, GGP and GGW) based on array-CGH. (a) Sporadic neuroblastomas: GGS vs GGP: $P=0.109$, GGS vs GGW: $P=0.320$ and GGP vs GGW: $P=0.002$. (b) Mass screening-detected neuroblastomas: GGS vs GGP: $P=1.000$, GGS vs GGW: $P=1.000$ and GGP vs GGW: $P=1.000$.

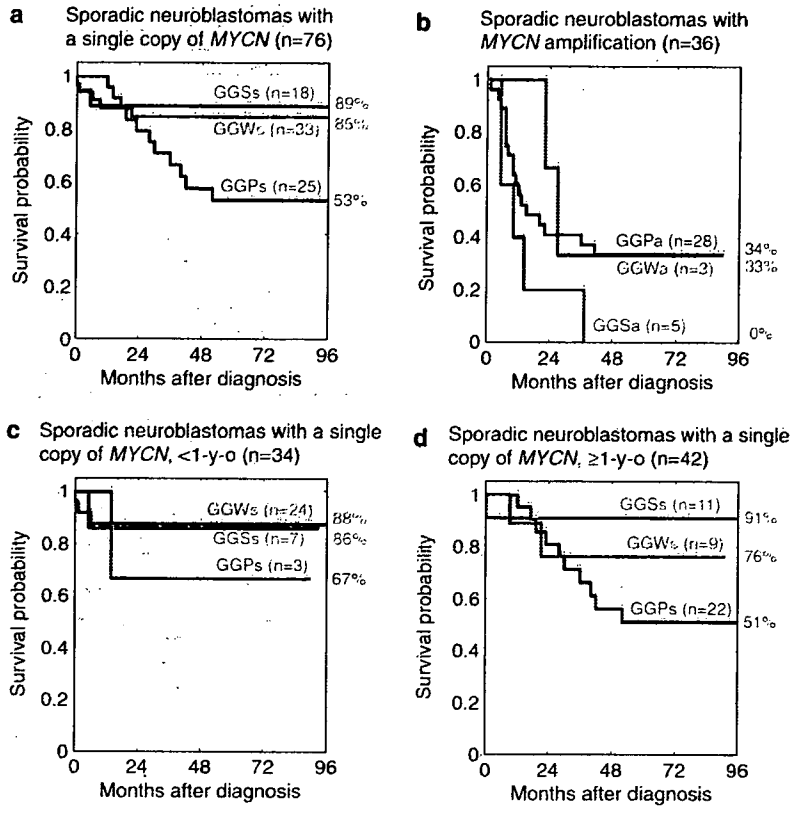

Figure 3 Kaplan Meier survival curves in three genomic groups (GGS, GGP and GGW) of sporadic neuroblastomas based on array-CGH. (**a**) Sporadic neuroblastomas with a single copy of *MYCN* GGS vs GGP: $P=0.035$, GGS vs GGW: $P=0.736$ and GGP vs GGW: $P=0.033$. (**b**) Sporadic neuroblastomas with *MYCN* amplification GGS vs GGP: $P=0.104$, GGS vs GGW: $P=0.156$ and GGP vs GGW: $P=0.642$. (**c**) Sporadic neuroblastomas with a single copy of *MYCN* in patients under 1 year of age GGS vs GGP: $P=1.000$, GGS vs GGW: $P=0.919$ and GGP vs GGW: $P=0.412$. (**d**) Sporadic neuroblastomas with a single copy of *MYCN* in patients over 1 year of age. GGS vs GGP: $P=0.063$, GGS vs GGW: $P=0.478$ and GGP vs GGW: $P=0.481$.

Discussion

The present array-CGH analysis revealed the whole feature of the genomic abnormality patterns of sporadic and MS-detected neuroblastomas. The patterns of genomic aberrations in MS-detected neuroblastomas are similar to those in sporadic tumors, suggesting that they are genetically genuine neuroblastomas which are similar to sporadic tumors found in patients under 1 year of age. Indeed, both of them have a high tendency to regress spontaneously. The exceptions we found are that the incidence of GGPs tumors is relatively higher in MS-detected tumors than in sporadic tumors found among young patients and that their clinical outcome is very good.

BAC array-based aCGH analyses have defined several minimal critical regions of gains and losses in 1p, 2p and 11q. These included minimal losses in 10 Mb regions of 1p36.3 (1pter to RP11-199O1, *D1S244*) and 11q23 (from RP11-42L18 to RP11-45N4). The 2 Mb region in 1p36.2--36.3 detected by a BAC clone RP11-219F4 (*D1S507*) exhibited highest deletion frequency of 32%. By combining the expression data obtained by the in-house microarrays harboring approximately 5340 genes derived from primary neuroblastomas, several candidate genes including *CHD5* at 1p36 (Bagchi *et al*., 2007) as well as *Survivin* at 17q25 (Islam *et al*., 2000) were identified as lowly and highly expressed genes in neuroblastomas with advanced stages, respectively (manuscript in preparation). The amplicon surrounding the *MYCN* locus was ranged from 2.4 Mb proximal (*G14110*) to 5 Mb distal (*D2S387*) of *MYCN* itself and gains were further extended to wider range, from 2pter to 2p11.

To date, the presence of the GGS subgroup with very silent aberrations of the tumor genome has never been verified definitely. The distribution of GGS tumors is very unique; namely, they are present in both MS detected and sporadic tumors removed from the patients under 1 year of age. They are also found in tumors obtained from the patients over 1 year of age, and some of them possess *MYCN* amplification. Furthermore, GGS tumors mostly show diploid karyotype. These facts suggest that GGSs tumors might represent neuroblastoma at an early stage of carcinogenesis with early oncogenic hit(s), which later develop to GGP or

Table 2 Univariate and multivariate analyses of genomic and molecular signature as well as other prognostic factors in sporadic neuroblastomas

	Sporadic NBLs (all cases)				*Sporadic NBLs (MYCN, single copy)*			
	N	P	*HR*	*CI*	N	P	*HR*	*CI*
Genomic signature (GGP vs GGW + GGS)	53 vs 59	0.003	2.59	(1.36, 4.90)	25 vs 51	0.010	3.41	(1.32, 8.82)
Molecular signature (posterior <0.5 vs ⩾0.5)	22 vs 18	<0.001	11.15	(2.52, 49.35)	13 vs 17	0.002	14.05	(1.72, 114.89)
Age (⩾1-year old vs <1-year old)	74 vs 38	0.006	2.67	(1.24, 5.77)	42 vs 34	0.070	2.47	(0.88, 6.96)
Stage (3, 4 vs 1, 2, 4s)	73 vs 38	<0.001	4.92	(1.93, 12.54)	38 vs 37	0.038	2.80	(1.00, 7.88)
Origin (adrenal vs nonadrenal)	72 vs 40	0.001	3.22	(1.43, 7.25)	41 vs 35	0.006	4.59	(1.33, 15.85)
TRKA expression (low vs high)	52 vs 36	0.004	3.37	(1.36, 8.34)	24 vs 36	0.766	1.21	(0.34, 4.31)
Shimada (unfavorable vs favorable)	39 vs 37	<0.001	4.54	(1.71, 12.07)	14 vs 36	0.668	1.37	(0.33, 5.75)
MYCN (amplification vs single copy)	36 vs 75	<0.001	3.98	(2.16, 7.35)				
Genomic signature (GGP vs GGW + GGS)	15 vs 25	0.045	2.89	(1.01, 8.30)	8 vs 22	0.031	5.46	(1.09, 27.40)
Molecular signature (posterior <0.5 vs ⩾0.5)	22 vs 18	0.002	7.52	(1.69, 33.38)	13 vs 17	0.034	7.41	(0.90, 60.87)
Genomic signature (GGP vs GGW + GGS)	53 vs 59	0.048	1.99	(1.05, 3.78)	25 vs 51	0.055	2.85	(1.10, 7.36)
Age (⩾1-year old vs <1-year old)	74 vs 38	0.132	1.88	(0.87, 4.06)	42 vs 34	0.549	1.44	(0.51, 4.05)
Genomic signature (GGP vs GGW + GGS)	53 vs 58	0.416	1.34	(0.71, 2.54)	25 vs 50	0.098	2.61	(1.01, 6.76)
Stage (3, 4 vs 1, 2, 4s)	73 vs 38	0.005	4.06	(1.60, 10.34)	38 vs 37	0.496	1.56	(0.56, 4.40)
Genomic signature (GGP vs GGW + GGS)	53 vs 59	0.012	2.23	(1.18, 4.23)	25 vs 51	0.015	3.19	(1.23, 8.26)
Origin (adrenal vs non-adrenal)	72 vs 40	0.006	2.78	(1.24, 6.26)	41 vs 35	0.008	4.30	(1.24, 14.88)
Genomic signature (GGP vs GGW + GGS)	41 vs 47	0.079	2.17	(0.96, 4.95)	18 vs 42	0.050	3.75	(1.06, 13.33)
TRKA expression (low vs high)	52 vs 36	0.078	2.34	(0.95, 5.79)	24 vs 36	0.727	0.79	(0.22, 2.80)
Genomic signature (GGP vs GGW + GGS)	53 vs 58	0.236	1.53	(0.81, 2.90)				
MYCN (amplification vs single copy)	36 vs 75	<0.001	3.30	(1.79, 6.08)				

Abbreviations: CI, confidence interval; GGP, partial chromosomal gains/losses genomic group; GGS, silent genomic group; GGW, whole gains and/or losses genomic group; HR, hazard ratio; *N*, sample number; NBLs, neuroblastomas; *P*, *P*-value.

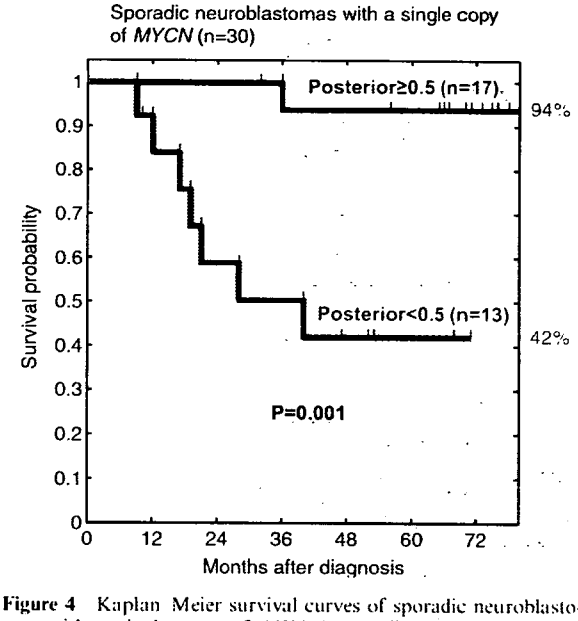

Figure 4 Kaplan Meier survival curves of sporadic neuroblastomas with a single copy of *MYCN* according to the molecular signature. Gene-expression profiling segregated patients into the favorable (posterior score⩾0.5) and unfavorable (posterior score<0.5) prognosis groups ($P = 0.001$). The posterior score denotes how likely the patient would show good outcome after 5 years (Ohira *et al*., 2005).

GGW tumors. Since MS did not decrease the incidence of sporadic neuroblastomas (Brodeur *et al*., 2001; Levy, 2005), GGSs tumors in young and old patients might be derived from different progenitor cells. It is interesting that the clinical outcome is very good for patients with *MYCN*-nonamplified GGSs tumors, whereas it is very bad for patients with GGSa tumors possessing *MYCN* amplification, implying again remarkable impact of *MYCN* amplification on the patient's outcome.

The GGP group is characterized by the presence of 17q gain with other chromosomal abnormalities including *MYCN* amplification, 1p loss and 11q loss. Since this group of tumors shows multiple chromosomal aberrations with partial gains and/or losses, unknown causes to induce genomic instability might have triggered genesis of neuroblastoma in progenitor or stem cells of sympathetic cell lineage (Maris and Matthay, 1999; Nakagawara, 2004). The frequently observed GGP tumors are as follows: GGP1a tumors with both 1p loss and *MYCN* amplification and GGP3s tumors with 11q loss but without *MYCN* amplification. The former may belong to a typical *MYCN*-amplified neuroblastoma (White *et al*., 1995) with a 5-year cumulative survival rate of 42% in our series, whereas the latter to the so-called intermediate type tumor (Srivatsan *et al*., 1993; Attiyeh *et al*., 2005) with the rate of 75%. In GGP tumors, it is obvious that *MYCN* amplification has the most powerful impact on the patient prognosis. Interestingly, among the GGPs tumors lacking *MYCN* amplification, 1p loss and 11q loss seem to similarly affect the prognosis. However, GGP2s tumors with both 1p loss and 11q loss show poorer prognosis in an additive manner. The similar additive effect has also been observed in GGP1a (42%

survival) and GGP2a (0% survival) with *MYCN*-amplified tumors. These suggest that 1p loss and 11q loss may independently affect the outcomes of neuroblastoma. Interestingly, one of the main characteristics of the *MYCN*-amplified tumors found in the long-term survivors is a lack of 11q loss (Supplementary Figure S4), corresponding to the observation that the high percentage of 5-year survival rate is shown in the GGP1a group with 1p loss but without 11q loss.

GGW neuroblastoma has a favorable prognosis, as reported (Vandesompele *et al.*, 1998). Since the pattern of chromosomal aberrations is represented by whole chromosomal gains and/or losses, mitotic dysfunction during the cell division cycle in progenitor or stem cells might have generated neuroblastoma (Maris and Matthay, 1999; Nakagawara, 2004). Interestingly, 1p loss or 11q loss in a minor population of GGWs tumors (GGW1s and GGW3s) seems not to affect the prognosis.

The presence of different patterns of genomic aberrations like GGS, GGP and GGW may reflect differences in stem or progenitor cells targeted to generate different genetic subsets of neuroblastomas. Although carcinogenic events to cause neuroblastomas may occur sequentially (Tonini, 1993), our serial analyses of six paired primary and recurrent tumors interestingly suggest that the major genetic events, for example, *MYCN* amplification, 1p loss, 11q loss and 17q gain, could occur not always in order during tumor progression (Supplementary Table S3).

Thus, the genomic signatures presented here successfully categorized new prognostic subgroups of neuroblastomas. The rather consistent patterns of genomic abnormalities provide reliable information to understanding of the genetic bases which underlie the clinical phenotypes of neuroblastomas with different survival rates. However, the pattern of genomic abnormalities may often lack biological significance affecting the clinical behavior of individual tumors. The gene-expression profile well reflects the biology of individual tumor. Therefore, establishment of the combined system of both genomic and molecular signatures is ideal for predicting the prognosis of individual patients with neuroblastoma. The present study has clearly shown that genomic and molecular signatures are independent prognostic indicators and suggests that an expression microarray could compensate for the relevant lack when used only genomic signature. In conclusion, combined genomic and molecular signatures may be clinically useful for constituting an ideal system to categorize and even individualize each tumor, which may make tailored medicine of neuroblastoma possible.

Materials and methods

Patients, tissue specimens and DNA/RNA resources

Tumor specimens were collected from 236 patients who had undergone biopsy or surgery at various institutions in Japan (see Supplementary Information). They included 112 sporadic and 124 MS-detected neuroblastoma specimens. All tumors were histopathologically diagnosed as neuroblastoma or ganglioneuroblastoma and were staged according to the International Neuroblastoma Staging System (Brodeur *et al.*, 1993). Informed consent was obtained at each institution or hospital. The procedure of this study was approved by the Institutional Review Board of the Chiba Cancer Center (CCC7817). Patients were treated by the standard protocols (Kaneko *et al.*, 2002; Iehara *et al.*, 2006) in Japan between 1995 and 2003. All MS-detected tumors were diagnosed between 6 and 8 months after birth by measuring urinary catecholamine metabolites in Japan (Sawada *et al.*, 1984). Fresh neuroblastoma tissues removed during surgery were stored at −80 C. *MYCN* copy number, *TrkA* mRNA expression and DNA ploidy were measured as reported previously (Islam *et al.*, 2000).

Microarray-based comparative genomic hybridization

A chip carrying 2464 BAC clones prepared by ligation-mediated PCR, which covers the whole human genome at roughly 1.2-Mb resolution (Snijders *et al.*, 2001; Albertson *et al.*, 2003), was used. The 500-ng aliquots of tumors and reference DNAs were labeled by random priming with each Cy3-dCTP and Cy5-dCTP (Amersham Pharmacia, Piscataway, NJ, USA). Hybridization was performed as previously reported (Pinkel *et al.*, 1998). UCSF Spot and UCSF Sproc programs to analyse values for spotted clones (Jain *et al.*, 2002) were used. All array-CGH data are available at NCBI Gene Expression Omnibus (GEO, http://www.ncbi.nlm.nih.gov/geo/) with accession number GSE 5784.

cDNA microarrays

In-house cDNA microarrays, carrying 5340 cDNAs obtained from the oligo-capping cDNA libraries generated from anonymous neuroblastoma tissues (Ohira *et al.*, 2003, 2005), were used. Preparation of RNA, hybridization, reading of spots and statistical analyses were conducted as reported previously (Ohira *et al.*, 2005). Gene-expression profile data described in this study is available at NCBI GEO with accession number GSE 5779.

Statistical analysis

The fluorescence ratio for each array CGH spot was normalized and rescaled into estimated copy number aberrations of each clone according to the comb-fit method (Oba *et al.*, 2006; see also Supplementary Figure S2a). Chromosomal events were detected by locally smoothing variations in copy number aberrations of clones on a chromosome and by applying threshold rules (see Supplementary Figure S2a and Supplementary Information for more detail). The numbers of whole chromosomal events, Nw and of partial chromosomal events, Np, were counted for 22 + 2 chromosomes in every specimen, and the scatter plot in the Nw Np plane exhibited apparent three clusters: whole differential dominant (Nw > Np), partial differential dominant (Nw < Np) and silent (Nw ≈ 0, Np ≈ 0) (Supplementary Figure S2b). To discriminate whole differential dominant from partial differential dominant, we defined a 'global' feature variable z as computationally evaluated as the ratio between Nw and Np; when z was small (large), the sample was likely to be whole (partial) differential dominant (see Supplementary Information for more detail). A differential analysis of gene expression was made using standard t-test with the q-value analysis (Storey and Tibshirani, 2003) for incorporating a false discovery rate (to deal with multiple statistical tests). A survival analysis was made based on Kaplan Meier and log-rank tests. Univariate and multivariate analyses were made according to the Cox hazard models.

Acknowledgements

We thank institutions and hospitals for providing tumor specimens (see Supplementary Information). We also thank Shigeru Sakiyama, Hiroki Nagase, Iwao Nozawa, Tadayuki Koda and technical staff, past and present, at Division of Biochemistry, Chiba Cancer Center Research Institute. We acknowledge Hisamitsu Pharmaceutical Co. Inc., the Ministry of Education, Culture, Sports, Science and Technology of Japan, the Ministry of Health, Labour and Welfare of Japan and the Hamaguchi Foundation for the Advancement of Biochemistry for funding this work.

References

Albertson DG, Collins C, McCormick F, Gray JW. (2003). Chromosome aberrations in solid tumors. *Nat Genet* **34**: 369–376.

Attiyeh EF, London WB, Mosse YP, Wang Q, Winter C, Khazi D *et al.* (2005). Chromosome 1p and 11q deletions and outcome in neuroblastoma. *N Engl J Med* **353**: 2243–2253.

Bagchi A, Papazoglu C, Wu Y, Capurso D, Brodt M, Francis D *et al.* (2007). CHD5 is a tumor suppressor at human 1p36. *Cell* **128**: 459–475.

Beckwith JB, Perrin EV. (1963). *In situ* neuroblastomas: a contribution to the natural history of neural crest tumors. *Am J Pathol* **43**: 1089–1101.

Brodeur GM. (2003). Neuroblastoma: biological insight into a clinical enigma. *Nat Rev Cancer* **3**: 203–216.

Brodeur GM, Look AT, Shimada H, Hamilton VM, Maris JM, Hann HW *et al.* (2001). Biological aspects of neuroblastomas identified by mass screening in Quebec. *Med Pediatr Oncol* **36**: 157–159.

Brodeur GM, Pritchard J, Berthold F, Carlsen NL, Castel V, Castelberry RP *et al.* (1993). Revisions of the international criteria for neuroblastoma diagnosis, staging, and response to treatment. *J Clin Oncol* **11**: 1466–1477.

Iehara T, Hosoi H, Akazawa K, Matsumoto Y, Yamamoto K, Suita S *et al.* (2006). MYCN gene amplification is a powerful prognostic factor even in infantile neuroblastoma detected by mass screening. *Br J Cancer* **94**: 1510–1515.

Islam A, Kageyama H, Takada N, Kawamoto T, Takayasu H, Isogai E *et al.* (2000). High expression of Survivin, mapped to 17q25, is significantly associated with poor prognostic factors and promotes cell survival in human neuroblastoma. *Oncogene* **19**: 617–623.

Jain AN, Tokuyasu TA, Snijders AM, Segraves R, Albertson DG, Pinkel D. (2002). Fully automatic quantification of microarray image data. *Genome Res* **12**: 325–332.

Kaneko M, Tsuchida Y, Mugishima H, Ohnuma N, Yamamoto K, Kawa K *et al.* (2002). Intensified chemotherapy increases the survival rates in patients with stage 4 neuroblastoma with MYCN amplification. *J Pediatr Hematol Oncol* **24**: 613–621.

Levy IG. (2005). Neuroblastoma, well-designed evaluations, and the optimality of research funding: ask not what your country can do for you. *J Natl Cancer Inst* **97**: 1105–1106.

Look AT, Hayes FA, Nitschke R, McWilliams NB, Green AA. (1984). Cellular DNA content as a predictor of response to chemotherapy in infants with unresectable neuroblastoma. *N Engl J Med* **311**: 231–235.

Maris JM, Matthay KK. (1999). Molecular biology of neuroblastoma. *J Clin Oncol* **17**: 2264–2279.

Nakagawara A. (1998). The NGF story and neuroblastoma. *Med Pediatr Oncol* **31**: 113–115.

Nakagawara A. (2004). Neural crest development and neuroblastoma: the genetic and biological link. *Prog Brain Res* **146**: 233–242.

Nakagawara A, Arima-Nakagawara M, Scavarda NJ, Azar CG, Cantor AB, Brodeur GM. (1993). Association between high levels of expression of the TRK gene and favorable outcome in human neuroblastoma. *N Engl J Med* **328**: 847–854.

Oba S, Tomioka N, Ohira M, Ishii S. (2006). Combfit: a normalization method for array CGH data. *IPSJ Trans Bioinformatics* **47**: 73–82.

Ohira M, Morohashi A, Inuzuka H, Shishikura T, Kawamoto T, Kageyama H *et al.* (2003). Expression profiling and characterization of 4200 genes cloned from primary neuroblastomas: identification of 305 genes differentially expressed between favorable and unfavorable subsets. *Oncogene* **22**: 5525–5536.

Ohira M, Oba S, Nakamura Y, Isogai E, Kaneko S, Nakagawa A *et al.* (2005). Expression profiling using a tumor-specific cDNA microarray predicts the prognosis of intermediate risk neuroblastomas. *Cancer Cell* **7**: 337–350.

Pinkel D, Segraves R, Sudar D, Clark S, Poole I, Kowbel D *et al.* (1998). High resolution analysis of DNA copy number variation using comparative genomic hybridization to microarrays. *Nat Genet* **20**: 207–211.

Sawada T, Hirayama M, Nakata T, Takeda T, Takasugi N, Mori T *et al.* (1984). Mass screening for neuroblastoma in infants in Japan. Interim report of a mass screening study group. *Lancet* **2**: 271–273.

Schwab M, Westermann F, Hero B, Berthold F. (2003). Neuroblastoma: biology and molecular and chromosomal pathology. *Lancet* **4**: 472–480.

Snijders AM, Nowak N, Segraves R, Blackwood S, Brown N, Conroy J *et al.* (2001). Assembly of microarrays for genome-wide measurement of DNA copy number. *Nat Genet* **29**: 263–264.

Srivatsan ES, Ying KL, Seeger RC. (1993). Deletion of chromosome 11 and of 14q sequences in neuroblastoma. *Genes Chromosomes Cancer* **7**: 32–37.

Storey JD, Tibshirani R. (2003). Statistical significance for genome-wide studies. *Proc Natl Acad Sci USA* **100**: 9440–9445.

Tomioka N, Kobayashi H, Kageyama H, Ohira M, Nakamura Y, Sasaki F *et al.* (2003). Chromosomes that show partial loss or gain in near-diploid tumors coincide with chromosomes that show whole loss or gain in near-triploid tumors: evidence suggesting the involvement of the same genes in the tumorigenesis of high- and low-risk neuroblastomas. *Genes Chromosomes Cancer* **36**: 139–150.

Tonini GP. (1993). Neuroblastoma: the result of multistep transformation? *Stem Cells* **11**: 276–282.

Vandesompele J, Van Roy N, Van Gele M, Laureys G, Ambros P, Heimann P *et al.* (1998). Genetic heterogeneity of neuroblastoma studied by comparative genomic hybridization. *Genes Chromosomes Cancer* **23**: 141–152.

Wei JS, Greer BT, Westermann F, Steinberg SM, Son CG, Chen QR *et al.* (2004). Prediction of clinical outcome using gene expression profiling and artificial neural networks for patients with neuroblastoma. *Cancer Res* **64**: 6883–6891.

White PS, Maris JM, Beltinger C, Sulman E, Marshall HN, Fujimori M *et al.* (1995). A region of consistent deletion in neuroblastoma maps within human chromosome 1p36.2–36.3. *Proc Natl Acad Sci USA* **92**: 5520–5524.

Woods WG, Gao RN, Shuster JJ, Robison LL, Bernstein M, Weitzman S *et al.* (2002). Screening of infants and mortality due to neuroblastoma. *N Engl J Med* **346**: 1041–1046.

Supplementary Information accompanies the paper on the Oncogene web site (http://www.nature.com/onc).

Oncogene (2008) 27, 741–754

www.nature.com/onc

ORIGINAL ARTICLE

Stress via p53 pathway causes apoptosis by mitochondrial Noxa upregulation in doxorubicin-treated neuroblastoma cells

K Kurata[1], R Yanagisawa[1], M Ohira[2], M Kitagawa[3], A Nakagawara[2] and T Kamijo[1,2]

[1]Department of Pediatrics, Shinshu University School of Medicine, Matsumoto, Nagano, Japan; [2]Division of Biochemistry, Chiba Cancer Center Research Institute, Chuoh-ku, Chiba, Japan and [3]Department of Biochemistry, Hamamatsu University School of Medicine, Hamamatsu, Shizuoka, Japan

In this study, we employed a panel of cell lines to determine whether p53-dependent cell death in neuroblastoma (NB) cells is caused by apoptotic cellular function, and we further studied the molecular mechanism of apoptosis induced via the p53-dependent pathway. We obtained evidence that a type of p53-dependent stress, doxorubicin (Doxo) administration, causes accumulation of p53 in the nucleus of NB cells and phosphorylation of several serine residues in both Doxo-sensitive and -resistant cell lines. Upregulation of p53-downstream molecules in cells and upregulation of Noxa in the mitochondrial fraction were observed only in Doxo-sensitive NB cells. Significance of Noxa in the Doxo-induced NB cell death was confirmed by Noxa-knockdown experiments. Mitochondrial dysfunction, including cytochrome-*c* release and membrane potential disregulation, occurred and resulted in the activation of the intrinsic caspase pathway. However, in the Doxo-resistant cells, the accumulation in the nucleus and phosphorylation of p53 did not induce p53-downstream $p21^{Cip1/Waf1}$ expression and the Noxa upregulation, resulting in the retention of the mitochondrial homeostasis. Taken together, these findings indicate that the p53 pathway seems to play a crucial role in NB cell death by Noxa regulation in mitochondria, and inhibition of the induction of p53-downstream effectors may regulate drug resistance of NB cells.
Oncogene (2008) **27**, 741–754; doi:10.1038/sj.onc.1210672; published online 20 August 2007

Keywords: neuroblastoma; p53; noxa; mitochondria; apoptosis

Introduction

Neuroblastoma (NB) is the most common pediatric solid malignant tumor derived from the sympathetic nervous system. Unlike the many childhood malignancies for which survival has been improved by recent therapies, high-risk NB is still one of the most difficult tumors to cure, with only 30% long-term survival despite intensive multimodal therapy. New treatments and a better understanding of drug resistance mechanisms are required for the improvement of the survival rate. A noteworthy finding of NB research is that mutations of p53 tumor suppressor have been reported in less than 2% of NBs out of 340 tested (Tweddle *et al.*, 2001). Instead of mutation, cytoplasmic sequestration of p53 has been proposed as an alternative mechanism of inactivation in NB cells. The sequestration was first detected in frozen tumor samples using immunohistochemical techniques (Moll *et al.*, 1995) and later in NB cell lines by immunofluorescence and cell fractionation experiments (Moll *et al.*, 1996). However, several groups reported nuclear p53 accumulation in NB cells harboring wild-type p53 after DNA damage (Tweddle *et al.*, 2003). After nuclear accumulation, p53 phosphorylation, binding to targeted sequences and transcriptional transactivation are sequentially induced by DNA damage in *p53* wild-type cells (Oren, 1999). However, these processes in NB cells harboring wild-type p53 have not been examined with respect to the role of p53 pathways in the tumorigenesis of NB. Their examination should also yield insights into the molecular mechanisms of p53 inactivation. For instance, upregulation of the p53-downstream genes encoding $p21^{Cip1/Waf1}$ and HDM2 in *p53* wild-type NB cell lines was observed in several studies (Isaacs *et al.*, 2001; Keshelava *et al.*, 2001; Tweddle *et al.*, 2001) but not all (Wolff *et al.*, 2001). Reporter gene assays detected p53 transcriptional function in one study (Keshelava *et al.*, 2001) but not in another (Wolff *et al.*, 2001). Together, these facts indicate that systematic and detailed analysis of the biological effects of p53-dependent stress on the cell death of NB cells and of the mechanisms of activation and signal transduction of p53-related pathways in NB cells are required for understanding the mechanism of drug resistance and for the development of new therapies for high-risk NB patients.

The Bcl-2 family member proteins regulate mitochondrial cell death by controlling mitochondrial outer membrane permeabilization (MOMP). Anti-apoptotic Bcl-2 family members (for example, Bcl-2, Bcl-xL, Bcl-w and Mcl-1) function to block MOMP, whereas the

Correspondence: Dr T Kamijo, Division of Biochemistry, Chiba Cancer Center Research Institute, 666-2 Nitona, Chuoh-ku, Chiba 260-8717, Japan.
E-mail: tkamijo@chiba-cc.jp
Received 4 December 2006; revised 1 June 2007; accepted 11 June 2007; published online 20 August 2007

various pro-apoptotic proteins promote it. The pro-apoptotic proteins fall into two general subfamilies, based on the sharing of Bcl-2 homology domains. BH123 proteins appear to be effectors of MOMP, because cells from mice lacking the two major BH123 proteins, Bax and Bak, fail to undergo MOMP in response to a wide range of apoptotic stresses (Wei *et al.*, 2001). The other subfamily, the BH3-only proteins, can act either to activate Bax or Bak or to interfere with the anti-apoptotic Bcl-2 family members (Letai *et al.*, 2002). Noxa is a BH3-only member of Bcl-2 family proteins (Oda *et al.*, 2003) and its expression is induced by DNA damage such as that caused by etoposide or doxorubicin in a p53-dependent manner (Oda *et al.*, 2003; Shibue *et al.*, 2003). Furthermore, several lines of evidence reported that Noxa is one of the most important cell death effectors in neuronal cell death, for example, nuclear factor-kappa B modulated cell death in mouse cortical neurons (Aleyasin *et al.*, 2004), axotomized motor neurons of adult mouse (Kiryu-Seo *et al.*, 2005), sensory neurons especially in trigeminal ganglia and cervical dorsal ganglia (Hudson *et al.*, 2005) and arsenite-induced cortical neurons (Wong *et al.*, 2005).

These results have led us to study the role and molecular machinery of p53-dependent cell death in NB by utilizing several *p53* wild-type NB cell lines. We studied the sensitivities of NB cell lines to doxorubicin (Doxo), which is a representative cytotoxic drug against NB cells (Matthay *et al.*, 1998) that induces stresses that are basically dependent on p53 (Lowe *et al.*, 1994), and transactivates p53 and its downstream effectors in many tissues (Komarova *et al.*, 1997). In sensitive NB cells, the following important findings were observed after Doxo treatment: (1) accumulation of p53 in the nucleus; (2) activation of the p53-downstream molecules; (3) pro-apoptotic BH3-only Bcl-2 family protein Noxa induction and upregulation in mitochondria resulting in mitochondrial dysfunction/intrinsic caspase-derived apoptosis. Although p53 accumulated in the nucleus before Doxo treatment, the downstream molecules were not induced and the upregulation of Noxa in mitochondria was not observed in the Doxo-resistant NB cells. Consequently, the crucial role of the p53 pathway in apoptosis in NB cells was indicated by our observations.

Results

Heterogeneity of response to p53-dependent death signals in NB cell lines harboring wild-type p53

We chose 0.5 μg/ml of Doxo as an appropriate concentration to assess the effect of Doxo on NB cells according to the results of the analysis of peak plasma concentrations of doxorubicin (Hempel *et al.*, 2002). Similar results were obtained by 0.3–1.0 μg/ml of Doxo in the following experiments (data not shown). Trypan blue uptake assays were performed to compare the Doxo sensitivity of NB cell lines harboring wild-type *p53* (Figure 1a). More than 60% of cells were Trypan blue-positive for the SH-SY5Y, NB9, NB69 and SK-N-SH NB cell lines 36 h after Doxo stimulation. On the other hand, less than 40% of cells were positive in NB-19 and NB1 cell lines and less than 10% in IMR32 cells even 36 h after Doxo stimulation.

Next, we performed WST-8 assay, a modification of MTT assay, to evaluate cytotoxicity on NB cells (Figure 1b). We confirmed the sensitivity of NB cells to Doxo by these experiments and also studied the effects of etoposide, the other p53-dependent damage-inducing reagent, on NB cells. Etoposide was effectively cytotoxic on the Doxo-sensitive SK-N-SH, SH-SY5Y, NB-9 and NB-69 cells. In the Doxo-resistant NB cells, IMR32 and NB-1 cells also possessed drug resistance against etoposide, whereas NB-19 cells had sensitivity.

FACS analysis of sub-G_0/G_1 cells showed that considerable percentages of cells underwent apoptosis 24 h after the Doxo treatment in SH-SY5Y, NB-9, NB-69 and SK-N-SH (Figure 1c). However, the proportions of apoptotic cells were significantly lower in NB-19, NB-1 and IMR32 than in the four Doxo-sensitive NB cell lines. In SK-N-SH and SH-SY5Y cells, the increase of the sub-G_0/G_1 fraction after Doxo treatment was confirmed by the condensation and fragmentation of nuclei (Figure 1d). In contrast, almost all of the nuclei were intact in the resistant IMR32 and NB-1 cells. Thus, Doxo-induced stresses resulted in apoptosis in some NB cells, whereas others were resistant (Figure 1).

Upregulation and nuclear accumulation of p53 are not enough to induce apoptosis by Doxo treatment

To study the basis of the different sensitivities of NB cells to p53-dependent stress, we first performed direct western blot analysis using a monoclonal antibody recognizing the p53 N terminus (DO1) to estimate the total amount of p53. We also used antibodies that specifically react with phosphorylated serine residues (Ser15, Ser20 and Ser46) to examine the modulation of the stability and/or activity of p53 in response to DNA damage.

The amount of p53 was clearly increased by Doxo in the Doxo-sensitive NB cells, as detected with DO1 antibody (Figure 2a). p53 accumulation was observed in the Doxo-resistant IMR32 and NB-19 cells before treatment; serine15 phosphorylation was induced in all the NB cells after Doxo exposure. Upregulation of serine46 phosphorylation was also observed in the NB cell lines, except for IMR32 and SH-SY5Y cells. On the other hand, ser20 phosphorylation was not strongly upregulated in any of the lines. Consistent with previous reports, RT–PCR analysis showed that the induction of p53 protein by Doxo treatment in sensitive-NB cells was not caused at the transcriptional level (Figure 2b). Thus, it appears that the upregulation of p53 protein in Doxo-treated NB cells seemed to be caused by protein stabilization.

Next, we investigated the localization of p53 in NB cells, using DO1 as a human p53-specific antibody reacting with amino acids 21–25, pAb421 as a pan-p53 antibody reacting with the human p53 amino acids 370–378 and